Automatic Gleason Grading of Prostate Cancer from Histological Images

Author

MUHAMMAD TAHIR FAROOQ

NUST201464494MCEME35214F

Supervisor

Dr. ARSLAN SHAUKAT

DEPARTMENT OF COMPUTER ENGINEERING
COLLEGE OF ELECTRICAL & MECHANICAL ENGINEERING
NATIONAL UNIVERSITY OF SCIENCES AND TECHNOLOGY
ISLAMABAD

MAY 2018

Automatic Gleason grading of Prostate Cancer from Histological Images

Author

MUHAMMAD TAHIR FAROOQ

NUST201464494MCEME35214F

A Thesis submitted in partial fulfilment of the requirements for the degree of
MS Computer Engineering

Thesis Supervisor:
Dr. ARSLAN SHAUKAT

Thesis Supervisor's Signature: _____

DEPARTMENT OF COMPUTER ENGINEERING
COLLEGE OF ELECTRICAL & MECHANICAL ENGINEERING
NATIONAL UNIVERSITY OF SCIENCES AND TECHNOLOGY,
ISLAMABAD

MAY 2018

Declaration

I hereby certify that this research work titled "Automatic Gleason grading of Prostate Cancer from Histological Images" is my own work under the sincere guidance of my supervisor Dr. Arslan Shaukat. The work has not been presented elsewhere for assessment. The material that has been used from other sources has been properly acknowledged / referred.

Signature of Student

MUHAMMAD TAHIR FAROOQ
NUST201464494MCEME35214F

Language Correctness Certificate

This thesis has been reviewed by an English language expert and is free of typing, syntax, semantic, grammatical and spelling mistakes. Thesis is also according to the format given by the university.

Signature of Student

MUHAMMAD TAHIR FAROOQ
NUST201464494MCEME35214F

Signature of Supervisor

Copyright Statement

Acknowledgements

Dedicated to my exceptional parents and adored siblings whose tremendous support and cooperation led me to this wonderful accomplishment

Abstract

Prostate Cancer (PCa) is one of the most common type of cancer found in men aged over 45 years. Detection and staging is the most critical step for pathologist and treatment decision is based on the findings. PCa is graded according to the Gleason grading criteria which is based on the glandular and pattern of the cells in the histological digitized biopsy slides. Manual grading depends on the experience of pathologists, quality of staining and some other parameters. To reduce these issues, an automatic grading system is required and this research will support the development of accurate computer aided design (CAD) system for the automatic detection and grading of prostate cancer. The goal of this study is to differentiate between benign and malignant tissues, classify the H&E stained histological images into one of the 3 grades as per Gleason grading criteria. Prostatic images data collection is the most challenging task in this research which took around 4 months. After visiting Shaukat Khanum Hospital several times, collected the H&E stained digitized images collected from around 150 patients. Dataset has been divided into four categories including grade 1-2, grade 3, grade 4 and grade 5 having 56, 69, 74 and 69 images respectively. In this research, we have extracted several features set using Gabor and local binary patterns (LBP) with its variants and combined the features to enhance the performance. We have applied multiple classifiers including K-Nearest Neighbours (KNN), Support Vector Machine (SVM) and Random Forest for evaluating performance. After analysing performance, we developed new features space by combining Gabor energy and rotation invariant LBP descriptors. It shows highest accuracy while having very low and simple feature dimensions. The proposed system shows overall average accuracy of 98.26 % while grading benign, grade 3, 4 & 5 grades.

Key Words: H&E *histological images, Gabor features, Gleason Grading, Local Binary Patterns, Prostate Cancer*

Table of Contents

List of Figures

List of Tables

CHAPTER 1: INTRODUCTION

The research work in this dissertation presents Computer Aided Diagnosis (CAD) system for detection and grading of prostatic cancer from the H&E stained images. This chapter explains the background, statement of problem, objective, scope, proposed methodology and evaluation of the Gleason grading technique. In the end of the chapter, thesis report organization is briefly explained.

1.1   Overview and Background

Prostate Cancer (PCa) or carcinoma of the prostate is the second common type of cancer above 40 years only found in men [1]. PCa develops with the uncontrolled growth of prostate glands in opposite to rectum and bladder. Prostate cancer is difficult to diagnose in the early stage as it has no clear symptoms in early stages. However, an early and correct diagnosis plays an important role in the treatment and life survival of the patient. Needle based biopsy tissue samples are considered the gold standard in diagnosis and grading of prostate cancer from which histopathological information is derived. Pathologists manually evaluate the samples under microscope and grade these samples according to Gleason grading. Gleason grading criteria is widely used and followed all over the world in clinical practice, which was endorsed by World Health Organization (WHO) in year 2003 for prostate carcinoma [2]. Gleason grading is based on glandular architecture of prostate developed by Dr. Donald Gleason in 1960s, which assigns grades to prostate cancer from 1 to 5 on the basis of histological structures (stroma, epithelial-cell nuclei, epithelial-cell cytoplasm and lumen) and architecture, where grade 1 shows initial stage and have differentiated uniform single glands and grade 5 shows the most aggressive stage and have anaplastic carcinoma patterns diffused prostatic stroma with minimal glandular differentiation [2]. In prostate cancer grading, importance is given to the higher grades (grade 3, 4, 5) as they are more aggressive and their grades must be marked by some expert pathologist team. Grade 1 and 2 normally represent benign or low-grade cancer, so these grades are not included in most of the studies.

Computer Aided Diagnosis or CAD is a new domain in medical practices which started with the advancement in digital slide scanners. In [4], authors insist on the importance of digital pathology and its role in diagnosis. CAD can save a lot of time and efforts of pathologists

because more than 80 percent of the tissues brought for diagnosis are benign. Computer based analysis plays an importance role in diagnosis because it can process millions of pixels which are visually invisible in a very short time which improves accuracy by reducing inter and intra-observer variations. It also aids in clinical research and helps in developing sound basis beneath any disease.

One of the major challenges in CAD systems is the enormous density of data which may comprise of 2.5 - 4 billion of pixels per slide from a single patient which is quite different from traditional radiographic images. CAD system needs to process a huge amount of data to work within multi-resolution framework. Another important outcome of computer aided image analysis is prognosis or detection of disease which may be based on prognostic markers. Thus, detection and staging of cancer became much expensive and complex process. Researchers agrees that computer analysis diagnosis is a very affective system based on detailed analysis approach considering tumour morphology and disease staging will lead to better treatment and patient care.

Figure 1.1 shows some H&E stained samples from the prostate cancer images database showing different patterns which define grade of the cancer. Figure 1.1 (a) shows benign sample as there is a well-defined cell pattern. In (b) Cells have no well-defined boundary but are isolated from each other, according to Gleason criteria it lies in grade 3 which is considered as low grade. (c) shows Grade 4 as it has cells overlapping and cell area has increased, also there are some patterns without defined boundaries. (d) shows grade-5 sample which is considered as last stage in Prostate cancer. There is no pattern as well as no boundaries, cells have lost all boundaries.

This thesis gives a detailed and comprehensive analysis of present state of the art techniques and approaches that have been implemented for Prostate cancer classification. Based on analysis of such approaches a novel, efficient and simple model is proposed for improved performance. First, the histological images database is collected from patients in the time span of about three months. Images database includes prostate cancer H&E histological images with different Gleason grades (1-5), few samples from the database are shown in figure 1.1.
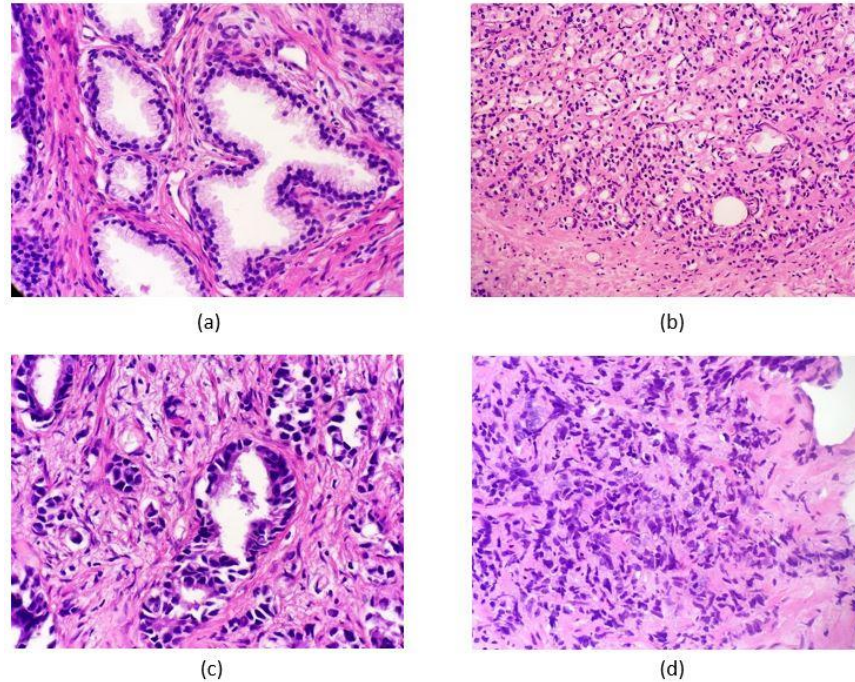
Figure 1.1: Prostate Cancer H&E samples

(a) Benign (b) Gleason Grade-3 (c) Gleason Grade-4 (d) Gleason Grade-5

After doing some pre-processing, several feature sets are extracted using Local Binary Patterns (LBP) with variants and Gabor wavelets by varying few parameters. K Nearest Neighbour (K-NN), Support Vector Machine (SVM) and random forest classifiers are utilized from WEKA toolkit [5] to evaluate performance of the proposed algorithm. Depending on the experiments performed, feature sets are combined to enhance the overall accuracy of the system. Performance of proposed system is then compared with the state of the art techniques in the literature and the results are discussed in results and experiments chapter.

1.2 Scope and Objective of Thesis

Our goal in this research is to collect real graded prostate cancer H&E stained database, detect the cancer or benign tissues and finally to grade the samples having cancer as per Gleason grading criteria. The computer aided detection and grading system is useful for further determining whether the gland is from a benign or a malignant tissue and if malignant then in what stage is it. Following are the key objectives of this research

We tend to develop a system that is intended to be used by physicians without getting into the complexity of algorithms being run in the background. This would motivate doctors in Pakistan to get assistance from Computer Aided diagnosis, hence saving their precious time, accordingly as the patient to Oncologist ratio in Pakistan is extremely low, many patients are bound to wait for a long span of time to get their turn, with the help of such software this time would be reduced. Other objectives are:

- To collect Prostate Cancer H&E images database from patients.
- To propose a new combination of descriptors based on analysis of most recent approaches of texture classification.
- To give a generalized descriptor that results in higher accuracy of classification on real prostate cancer images dataset.
- To reduce feature set dimensionality.

1.3 Contributions

We have collected cancer real images from Shaukat Khanum Memorial Cancer Hospital & Research Centre Lahore, Pakistan. An extensive range of research has been conducted on detection and staging of prostate cancer. We have extracted number of feature sets from the dataset and applied a series of classifier to evaluate the overall performance of the system. Proposed approach outperformed in terms of detecting and staging cancer according to Gleason grading on both the web pathology dataset and real datasets.

1.4 Organization of Thesis

The thesis is organized as follows:

- Chapter 2 discusses the clinical background of colorectal cancer, its diagnosis procedures, importance of histopathology and procedure starting from slide preparation till digitization of slide.

- Chapter 3 covers the literature review of Prostate cancer, detection and Gleason grading of histological images.

- Chapter 4 covers the proposed methodology of the computer aided grading system with the help of its mathematical models and graphical representations.

- Chapter 5 covers the quantitative and pictorial results obtained through the proposed methodology.

- Chapter 6 discusses the conclusion and future recommendations.

CHAPTER 2: BACKGROUND RELATED TO PROSTATE CANCER

This chapter describes in detail the cancer as disease of cells, clinical findings, cancer statistics, symptoms and causes of prostate cancer. Slide preparation, chemical staining and digitizing of slides for computer aided diagnosis is discussed. In last section of the chapter, Gleason grading of Prostate samples is discussed in detail with the unique features to differentiate between different grades.

2.1 Cancer: A Disease of Cells

Millions of cells growing, dividing and dying in a conventional manner are present in a human body. In a normal human body, growth of cells is a completely controlled process. But sometimes due to some reasons, cells growth goes uncontrolled which leads to cancer. Cancer cells combine and form huge tissues called tumor [6]. Cancer is disease which spread through blood flow in human body. Not all tumors spread throughout the body but they grow uncontrollably like benign tumor [7]. Growth of healthy cells is completely controlled and if healthy cells get unhealthy they are destroyed by themselves.

Researchers in the field are not yet able to find some specific cause for cancer. Cancer cells are highly modulated by the microenvironmental and culture conditions [7]. There are multiple factors which increase the risk of cancer such as intake of alcohol, tobacco, unhygienic food, exposure to ultra violet (UV) radiation and lack of physical activities [6].

2.1.1 Benign Growths

Benign tissues or benign prostatic hypertrophy are almost no threat to life. Benign growth shows following characteristics [8]

- Don't invade or effect the tissues in neighbours
- Don't spread to other parts or organs of body
- Can be removed by surgery and normally not grow back

2.1.2 Malignant Tumors

The malignant tumors are named same as benign tumors, with certain additions and exceptions which are [9]

- Malignant neoplasms of epithelial cells are called carcinomas regardless of the tissue of origin. Thus, a malignant neoplasm arising in the renal tubular epithelium (mesoderm) is a 20 carcinoma, as are the cancers arising in the skin (ectoderm) and lining epithelium of the gut (endoderm)

- Carcinomas are subdivided further. Those relevant to this research are prostatic which grow in a gland like pattern are referred as adenocarcinomas. Therefore, the cancer that arises in prostate exhibits glandular patterns.

2.1.3 Cancer Statistics

Cancer is one of the most dangerous and killer disease with several types found in both males and females. Among all cancers, Prostate cancer is the second biggest killer disease after lung and bronchus cancer in males. Prostate cancer results in about 25,000 deaths each year in United States and [1] reports 26,120 deaths in year 2016 out of 180,190 registered cases. It is about 21% of the total cancer found in men around the world. This makes 15% of cancer related death cases, second to lung cancer. More cases are registered in US, Canada, New Zealand, Australia, Sweden and other developed countries then in less developed countries [3]. Facts and figures regarding prostate cancer by American cancer society are summarized in figure 2.1 below. Accordingly, we can see that mortality as well as cancer incidence is more common in men then in women.

Males			Females		
Lung & bronchus	85,920	27%	Lung & bronchus	72,160	26%
Prostate	26,120	8%	Breast	40,450	14%
Colon & rectum	26,020	8%	Colon & rectum	23,170	8%
Pancreas	21,450	7%	Pancreas	20,330	7%
Liver & intrahepatic bile duct	18,280	6%	Ovary	14,240	5%
Leukemia	14,130	4%	Uterine corpus	10,470	4%
Esophagus	12,720	4%	Leukemia	10,270	4%
Urinary bladder	11,820	4%	Liver & intrahepatic bile duct	8,890	3%
Non-Hodgkin lymphoma	11,520	4%	Non-Hodgkin lymphoma	8,630	3%
Brain & other nervous system	9,440	3%	Brain & other nervous system	6,610	2%
All Sites	314,290	100%	All Sites	281,400	100%

Figure 2.1: Ten Leading Cancer types causing deaths [1]

		Males	Females		
Prostate	180,890	21%	Breast	246,660	29%
Lung & bronchus	117,920	14%	Lung & bronchus	106,470	13%
Colon & rectum	70,820	8%	Colon & rectum	63,670	8%
Urinary bladder	58,950	7%	Uterine corpus	60,050	7%
Melanoma of the skin	46,870	6%	Thyroid	49,350	6%
Non-Hodgkin lymphoma	40,170	5%	Non-Hodgkin lymphoma	32,410	4%
Kidney & renal pelvis	39,650	5%	Melanoma of the skin	29,510	3%
Oral cavity & pharynx	34,780	4%	Leukemia	26,050	3%
Leukemia	34,090	4%	Pancreas	25,400	3%
Liver & intrahepatic bile duct	28,410	3%	Kidney & renal pelvis	23,050	3%
All Sites	**841,390**	**100%**	**All Sites**	**843,820**	**100%**

Figure 2.2: Ten Leading Cancer types for the estimated new cancer cases [1]

Figure 2.1 and 2.2 shows ten leading cancers expected cases and deaths in men and women [1]. Prostate cancer accounts for 21% in men making it the second cause of death in men fighting cancers as shown in figure 2.1. The need for computer aided prostate cancer grading system can be observed from figure 2.2 according to which Prostate cancer is the most reported cancer in men. In manual grading, pathologists repeat complete procedure multiple times while grading the sample as benign or malignant. If malignant, then sample is graded according to Gleason grading criteria which is a lengthy process. Due to large number of new expected Prostate cancer cases, there is high probability of errors and large time is required to manually grade the sample. The research on the diagnosis and treatment of prostate cancer is increasing on an enormous rate due to increase in the number of new cases. Due to increase in the number of patients around the globe, an authentic and precise system is required for detection and grading of the histological images. In this chapter, we would discuss the clinical background of Prostate cancer.

2.2 Introduction to Histology

Histology is referred as study of the tissues and arrangement of tissues to constitute different organs. Histology involves all characteristics regarding biology of tissue structure, it emphasizes on cell arrangement which combine in different patterns to form tissues which optimize functioning relevant to different organs [5]. The most important procedure before the study of any histological structure is the preparation of tissue sections or slices that can be studied with the light microscope. Under the light microscope, tissues are examined visually in a beam of transmitted light. Tissues are required to be sliced in form of thin translucent sections that may

be attached to glass slides to examine under light microscope, this step is crucial because most tissues and organs are too thick for light to pass.

2.2.1 Preparation of Slides

Following are the basic steps that are required for preparation of slides before analysis [11] as shown in figure 2.3.

Figure 2.3: Slide preparation procedure [11]

- *Fixation:* preservation of cross-linking proteins and inactivation of enzymes that break down the tissues is done by placing small tissue in solution of different chemicals

- *Dehydration:* water removal is done by passing it through different concentration of alcohol.

- *Clearing:* Alcohol is removed from above.

- *Infiltration:* The tissue is afterwards placed in molten paraffin till paraffin is penetrated in it.

- *Embedding:* tissue from the previous step is placed in a small mold so that it may harden

- *Trimming:* The resulting paraffin block is pruned so that it may be used for further sectioning.

2.2.2 Staining of Slides

For precisely distinguishing microscopic tissue components, slides need to be stained and dyed. This is to be done to improve distinction and to make the tissue components more visible. Examples of frequently used dyes are Alcian blue, methyl blue and toluidine blue. The most

common dye out of these is H&E (Haematoxylin and Eosin). Haematoxylin stain basophilic and Eosin stain acidophilic components, as these are acidic and basic dyes respectively. DNA in the nuclei of cell and cytoplasm are high in pH so Haematoxylin stains them dark blue, while Eosin stains acidic components like collagen pink [11] .

2.2.3   Digitization of slides

With the evolution in Computer Aided Diagnosis, digitization of slides is done using high tech slide scanners. Digitization of histological sections into whole-slide images (WSIs) can be done by a Zeiss MIRAX MIDI slide Scanner. The WSIs were subsequently rescaled to a pixel resolution of 0.620 μm (equivalent to 20x magnification) which is normally used. Image digitization is done using - Carl Zeiss Microimaging Inc., MIRAX MIDI. With its innovative horizontal loading system, the MIRAX MIDI offers a method of reliably digitize freshly cut slides [12].

Figure 2.4: Mirax Image Digitizer

The MIRAX MIDI combines excellent image quality and high scan speed in a compact and accessible design. This facilitates scanning of slides in up to 10 different fluorescence channels in parallel through its fluorescence mode, therefore MIRAX MIDI is ideal for both hybridization applications as well as immunofluorescence applications. Figure 2.4 shows the MIRAX MIDI scanner.

2.3   The Prostate Cancer

The prostate is a part of a men reproduction system, situated before the rectum under the bladder. The prostate encompasses the tube through which urine passes also known as urethra. The size of normal prostate is approximately equal to the size of walnut. If the size of prostate gets too large, it compresses the urethra which will slow or stop the flow of the urine. Prostate is an organ which helps in making of seminal liquid. During orgasm, seminal facilitate semen to flow out of the body.
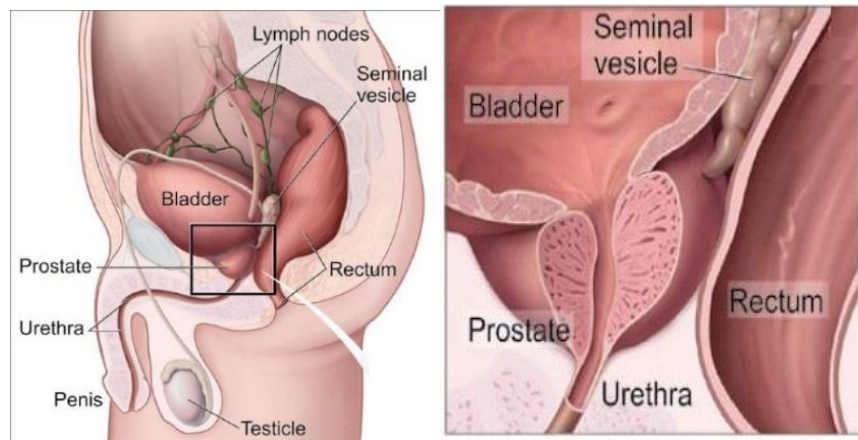
Figure 2.5: a) Prostate and nearby organs   b) Urethra surrounded by prostate [11]

Figure 2.5 shows the structure of Prostate in healthy human male which exist between rectum and bladder. A healthy prostate weight around 11-16 grams [12] and situated between Rectum and bladder. If the size of the prostate increases, it can press the urine tube and patient will face severe pain in urination. The prostate only exists in males and it normally grows with the age, if it grows to a threshold then it will create blockage in the urination process. There are few symptoms of prostate cancer which are discussed in next section.
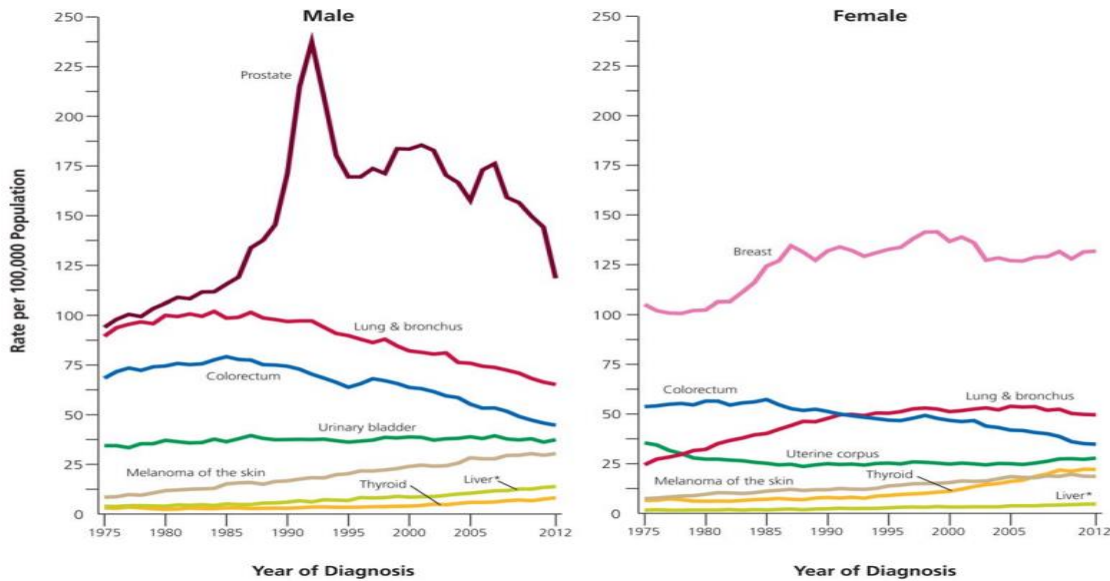
Figure 2.6: Trends in incidence rates for selected cancers from year 1975 to 2012 [1]
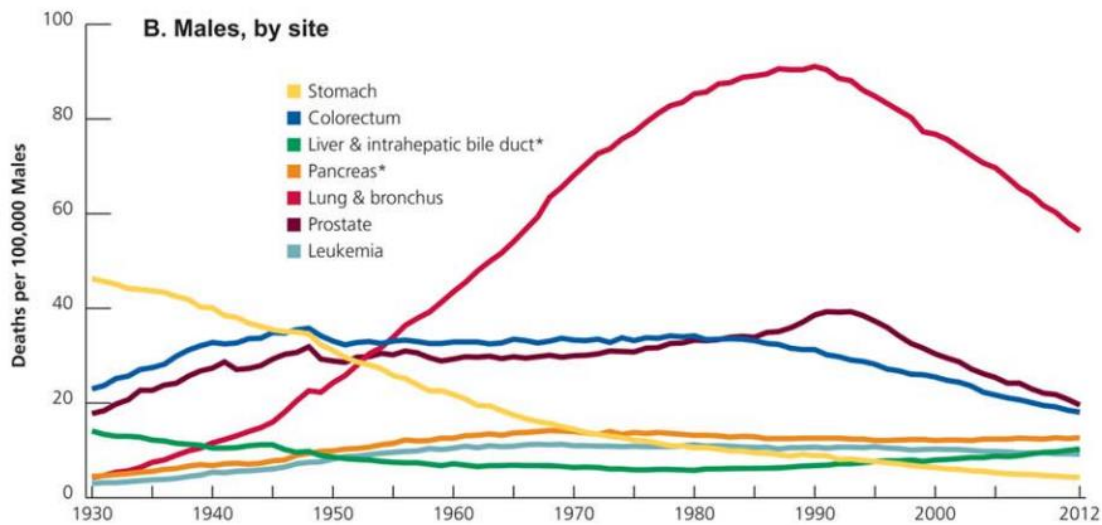
Figure 2.7: Deaths due to cancer by population in males from year 1930 to 2012 [1]

Figure 2.6 graphs shows stats of males and females patients effected by different cancers in the period from year 1975 to 2012 taken from [1]. The vertical axis is divided on rate per 100,000 population, Prostate cancer in males and breast cancer in females are highly diagnosed cancers. Figure 2.7 shows the number of deaths due to cancer types by population in males from year 1930 to 2012. The graph shows that highest death rate is due to lung and bronchus cancer. Prostate cancer is the second largest deadly cancer found in males as shown in figure 2.7.

12

2.3.1 Symptoms of Prostate cancer

Prostate gland lies near bladder and urethra so it can mostly be diagnosed by urinary symptoms. The tumor may press or constrict the urethra depending on the size and location which will affect the flow of the urine.

Due to increase in the size of the prostate tumour, urination may be affected. Some of the symptoms related to urination are [10]:

- Burning pain during urination

- Difficulty in urinating

- Troubles in starting or stopping of urine.

- Frequent urination in the night

- Almost no control on bladder

- No continuous urine stream

- Sometimes blood in urine (hematuria)

Prostate cancer may be spread by metastasize to bones or tissues. If cancer starts spreading and start effecting the spine, then spiral nerves can be pressed. A patient may get following symptoms:

- Blood can be seen in semen

- Difficulty in erection or erectile dysfunction

- Severe pain during ejaculation

- Legs swelling or in pelvic area

- Pain or numbness in the legs, feet or hips

- Severe pain in bones leading to fractures.

2.3.2 Grading of Prostate Cancer

Prostate Cancer (PCa) or carcinoma of the prostate is the second common type of cancer only found in men [1] aged above 40 years. Prostatic sample is assigned one of the 5 grades depending on the histological structures (stroma, epithelial-cell nuclei, epithelial-cell cytoplasm and lumen) and architecture as shown in figure 2.8. Grade 1 shows initial stage and have differentiated uniform single glands and grade 5 shows the most aggressive stage and have diffused prostatic stoma with minimal glandular differentiation level [13]. Figure 2.8 shows in depth analysis of all five Gleason grades with real H&E prostate cancer tissue samples. In grading process, higher grades (grade 3,4,5) are critically focused due to their high aggressiveness.
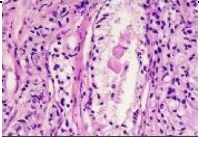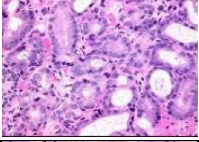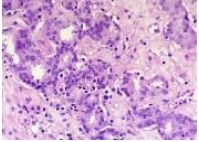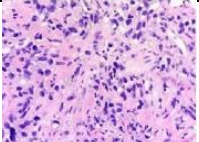
Grade	Pattern Description				Gleason Pattern Sample
	Tumor Boundary	Pattern	Size	Spread	
1	Sharp boundaries	Well differentiated uniform single glands which grows almost together	Medium	Closely packed	
2	Less well circumscribed	Variably spaced single glands apart and boundaries of the tumor are not finely bounded	Medium	Upto one gland diameter apart	
3	Well circumscribed	Single, irregular, separate, round or large masses with papillary pattern	Small to large	Loosely packed with well-defined margins	
4	Architecture lost	Fused gland tumor, mostly consist of pale cells	Small or medium	No individual or separated glands	
5	Minimal glandular differentiation	Comedo carcinoma tumors and cords, solid sheets with no acinar formation	Small	Diffusely infiltrating prostatic stroma	

Figure 2.8: Gleason Grading features with H&E images samples

The health condition and life of patient is mostly dependent on the Grading accuracy therefore, only team of expert pathologist should mark the grades. Grade 1 and 2 normally represent benign or low-grade cancer, so these grades are not included in most of the studies.

Pathologists evaluate Gleason score manually by observing the H&E stained glass tissues under microscopes [13]. Whole slide may show multi-grades therefore, slide in divided into sub-slides and then score is calculated by adding different scores present. Visual assessment of whole slide images is a time-consuming process and is highly dependent on the inter and intra-observer variation of the pathologist. In manual diagnosis and grading of prostate cancer, there is a high probability of under-grading or over-grading. Under grading refers to identifying higher grade as lower and over grading refers to identifying low grade as high grade. Under grading is a serious problem as it will change the treatment of higher grades (grade 4 or 5) to the treatment of low grades (grade 1,2) which will badly effect the condition of the patient. These issues call for some automatic detection and grading system of prostate cancer with improved accuracy.

2.4   Summary

This chapter is divided into three major sections as clinical findings of Prostate cancer, chemical staining, slides digitization process and prostate cancer grading criteria. Difference between benign and malignant tissues are described. Leading cancer types and reported deaths caused by cancers in males and females are described with the reported statistics. Common causes and symptoms of prostate cancer are briefly described. The second section of the chapter discusses step by step process of preparing and staining slides. These slides are then digitized to support computer aided systems for grading. Gleason grading criteria is also discussed in tabular form with real digitized slide images from the dataset.

CHAPTER 3:   LITERATURE REVIEW

Tissues are made up of cells and cells distribution in any organ has normally some specific texture pattern. The natural texture pattern help pathologist to differentiate between healthy and abnormal tissues. An extensive research exists in literature on texture analysis covering machine vision and image processing areas from biomedical to industrial, image classification to image segmentation, object detection to recognition. Most researchers in this area focused on feature extraction from medical images to develop a precise computer aided system for cancer detection and classification. This chapter discusses computer aided systems, Prostate cancer grading and Gleason grading literature and a brief research overview in this domain.

3.1   Computer Aided Diagnosis (CAD) Systems and Digital Pathology

In recent years, Computer Aided Diagnosis (CAD) systems have been developed for medical applications. The trend started after the advent of digital slide scanners. Few research papers that insist on the importance as well as limitations of CAD systems are mentioned here. In [14], authors insisted on the importance of digital pathology and its role in diagnosis. CAD helps in saving a lot of time and effort of pathologists as more than 80 percent of the tissues brought for diagnosis are benign. The computer based analysis shows better performance in term of accuracy and time consumed due to very less human interference. It also aids in clinical research and helps in developing sound basis beneath any disease.

Principle challenge in CAD is the enormous density of data which comprises of 2.5 - 4 billion pixels per slide, so unlike traditional radiographic images CAD for histopathological images works within multi-resolution framework. Another important usage of computer aided image analysis is   prediction of disease based on prognostic markers. Therefore, it become challenging task to have precise predictors for CAD system. According to researcher, a computer aided image analysis considering tumor morphology and disease subtypes will lead to better patient care. Cooper Carter [4] outlines history of microscopy, influence of diagnostics and introduced image digitization in the field of pathology. They also reported some state of art techniques related to computerized medical analysis. Normally medical images have high pixels density which sometime become a challenge for real time processing. Computational cost of

CAD systems in pathology is high, authors highlighted this issue to reduce and proposed different techniques to reduce the cost as intelligent memory utilization.

Using image processing knowledge for diagnosis, literature shows researchers have utilized multiple methodologies to achieve different goals as extracted features based classification, image registration, region and object segmentation with the development in Computer Aided Diagnosis, pathological diagnosis entered a new era. Now digital diagnosis is consider much precise and is used on large scale in diagnosis of prostate cancer [15], cervical cancer [16], breast cancer [17], neuroblastoma [18] and colon cancer [19].

3.2   Texture Analysis for Cancer

For detection and classification of cancerous or benign tissues in cancer, the texture layout of the stained image is most important. The gold standard used as standard around the globe is based on the architectural details of the stained image [13]. For this reason, it is very important to review some literature on texture feature extraction and classification. Several feature extension and analysis techniques have been proposed in literature [20]. Some of the mostly used texture classification methods are studied, analysed and compared for outstanding performance. Researchers performed textural classification with minor changes in already implemented algorithms and gradually got better results. Research overview regarding texture classification is presented here in different divisions based on feature extraction techniques.

An extensive analysis of textures for image segmentation have been conducted in literature for medical imaging. Texture analysis plays an important role in partitioning an image into several meaningful sub images. Several techniques and tools have been proposed for texture features extraction. Segmentation is considered as key towards image analysis and its higher activities such as compression, visualization, medical diagnoses, scene analysis and other applications. Texture based image segmentation started with the introduction of texture and scene imaging. In late 70s, Sklansky and Jack [21]   published his work on image segmentation proposing textures and boundary detection for features extraction. He explained and analysed textures and its features in details along with shape descriptors and spatial relations. Haralick [22] presented a survey on several approaches of texture features extraction including statistical and structural techniques.

17

Waught [23] used texture analysis (TA) for classification of breast cancer through MRI images, the research was based on the texture analysis. Research by Xie, et al., [24] and Chang-ming, et al., [25] worked out on segmentation of texture based ultrasound images. The former one utilized texture and shape priors for segmentation of kidney ultrasound images. They presented a supervised segmentation for the extraction of organs of interest from ultrasound images. Segmentation is done using both shape and texture priors. In training phase shape model is constructed using dataset of training shape and two-sided texture patterns are created using Gabor filters bank. Gabor filters bank are also applied on two sides of the curve using two-sided convolution strategy to get texture features of inside and outside regions. Based on texture features, texture measures are calculated and the texture energy functions are then minimized using optimization algorithms. The technique is evaluated by applying on both natural images and clinical images. Applications of their methodology are also used for the segmentation of kidney ultrasound images and results are compared with other segmentation methods.

3.3   Prostate Cancer Classification

Fehr et al. [35] presented multiple machine learning and feature selection for classifying benign and malignant prostate cancer tissues with accurate grades. Authors claimed that results suggested much accurate classification with high sensitivity and specificity. Due to unavailability of publicly available prostate dataset results couldn't be compared with other techniques. The authors showed that combining selected image features followed by Support Vector Machine (SVM) classification showed highest classification rate. Almuntashri [30] presented a CAD system for Gleason grade of prostate cancer H&E stained pathological images. The introduced algorithm combines features from Features extracted by using fractal analysis and wavelet transform are combined. The grading system achieved an average Gleason grading accuracy of 95%. The system was trained and tested on dataset of 45 images with different resolution, stain colors, magnification levels. Epstein et al. [36] proposed a new grading system by defining the Grading patterns and criteria. A team of more than 65 pathology experts including 17 clinicians from 19 different countries created a new grading system.

Rezaeilouyeh et al. [26] used Shearlet transform feature coefficients, color channel histogram and morphological features. Applied Support Vector Machine (SVM) classifier after concatenating the feature set for improved accuracy. Maximum accuracy of 90% achieved on

dataset of 100 H&E histological images. Litjens et al [27] used super pixel and Local Binary Patterns (LBP) features. Random Forest tree classifier with 10 folded cross validation was used. Achieved maximum accuracy of 90% with images dataset of 204 images from 163 patients. Desktop computer took around 5 minutes to detect the cancer in the slide images. Mosquera [2] used combination of wavelet and fractal analysis to get unique feature sets. Pairwise coupling SVM classifier is used with 3 different cross validations which results in 89% accuracy for prostate cancer Gleason grading. Lopez [28] proposed a system by integrating gland architectural and morphology features, capable of grading samples in grade 3, 4 or 5. Khurd [29] performed cell segmentation and computed a network model by locating cell locations on a dataset of 45 H&E images.

Hong-Jun [31] extracted Haar wavelet energy and fractal dimensions. 45 prostatic images with different resolution, magnification and stain colours are used for validating the proposed system which results in 95% accuracy. Khurd [15] have developed a texture based classification system. Texture is extracted by the system at pixel level into basic texture element called textons. Then random forest classifier is used for classification in conjunction with SVM. Proposed system is capable of distinguishing between Gleason grades 3 and 4. Cheng-Yi [32] used fractal dimensions for feature set and applied SVM and Leave-one-out manner. Algorithm is tested on total 1000 images which are collected over a period of 5 years and claimed accuracy of 86.3%. Gertych et al. [33] extracted intensity based features histogram and combined local binary pattern features with local variance features, used support Vector Machine (SVM) followed by Random forest classifier to classify the images into benign or malignant tissues. Tabesh et al. [34] extracted color, texture and morphological features and combined all for high classification rate. Authors showed cancer detection rate of 95% and Gleason classification rate of 81% on prostate images dataset.

Gabor was widely used in applications as machine vision, image processing and pattern recognition. The major advantage of Gabor filter is that it shows optimum characteristics in both frequency and spatial domains [37]. Hassan [38] proposed a novel approach to scale and rotation invariant. The proposed approach is based on Gabor filters. Homogenous Texture (HT) features are extracted in form of two independent matrices means and variance. Authors used Gabor filter with 6 orientations and 4 scales. Comprehensive and detailed analysis of LBP and its most recent extensions were compiled by M. Pietikainen in the form of a book published by Springer [39]. Detailed overview of LBP

operators with variants were presented for features extraction, computational complexity, performance and mathematical modelling. First section of the book describes utilization of LBP operator for still images, also its applications in textures such as retrieval, segmentation, classification, region of interest description and detection of objects. Applications of LBP operators in dynamic textures, recognition and motion analysis was also described.

3.3.1 Gleason Grading for Prostate Cancer

Gleason grading is based on glandular architecture of prostate developed by Dr. Donald Gleason in 1960s, which assigns grades to prostate cancer from 1 to 5 on the basis of histological structures (stroma, epithelial cell nuclei, epithelial-cell cytoplasm and lumen) and architecture, where grade 1 shows initial stage and have differentiated uniform single glands and grade 5 shows the most aggressive stage and have diffused prostatic stoma with minimal glandular differentiation level [3].

Gleason Grading features with H&E images samples are shown in previous chapter in figure 2.8. The grading system was modified in 1977 and notified by [40] for needle based biopsy samples. The modifications are reported in detail in table 3.1 below. It is remarkable that after 50 years, Gleason grading remains one of the most powerful cancer predictor for needle based biopsy samples. But with the passage of time and improvements in pathology, slight modifications were made and reported by Jonathan I. Epstein [40].

Table 3-1: Gleason System [40]

Original Gleason System: 1966 & 1967
Pattern 1: Very well differentiated, small, closely packed, uniform, glands in essentially circumscribed masses
Pattern 2: Similar (to pattern 1) but with moderate variation in size and shape of glands and more atypia in the individual cells; cribriform pattern may be present, still essentially circumscribed, but more loosely arranged
Pattern 3: Similar to pattern 2 but marked irregularity in size and shape of glands, with tiny glands or individual cells invading stroma away from circumscribed masses, or solid cords and masses with easily identifiable glandular differentiation within most of them
Pattern 4: Large clear cells growing in a diffuse pattern resembling hypernephroma; may show gland formation
Pattern 5: Very poorly differentiated tumors; usually solid masses or diffuse growth with little or no differentiation into glands
Gleason's Modifications: 1974 & 1977
Patterns 1 & 2: Unchanged
Pattern 3: Adds to earlier description: may be papillary or cribriform (1974), which vary in size and may be quite large, but the essential feature is the smooth and usually rounded edge around all the circumscribed masses of tumor (1977)
Pattern 4: Adds to earlier description: raggedly infiltrating, fused-glandular tumor (1974); glands are not single and separate, but coalesce and branch (1977)
Pattern 5: Adds to earlier description: can resemble comedocarcinoma of the breast (1977); almost absent gland pattern with few tiny glands or signet cells (1977)

3.4   Summary

This chapter describes the research literature overview regarding computer aided diagnosis for digital pathology, prostate cancer classification, Gleason grading criteria and the modifications. Different techniques, approaches and descriptors are briefly described which are implemented in literature for different texture applications. Feature extraction by Gabor filters and local binary patterns are explained in accordance with the literature.

.

CHAPTER 4:   PROPOSED METHODOLOGY

This chapter describes in detail our methodology that we have used for Gleason grading of H&E prostate cancer images. Chapter is divided into three major sections as Data Acquisition, Feature extraction and fusion, Classification. Each section is discussed in detail with the help of mathematical modelling. Experimental setup & cross validation method is also discussed in the end of the chapter.

4.1   Proposed System overview

Accuracy of any image classification system depends on the uniqueness of features or patterns that have been extracted to perform classification in noisy environments [42]. Classification algorithm cannot be trained or tested fairly without having handsome number of images in dataset in terms of quality and quantity. However, different applications may require different feature descriptors for better classification rate. Extensive research has been carried out in literature to get appropriate features to achieve better classification results for different applications. In this thesis, we have proposed to develop a Prostate Cancer Gleason Grading system using Gabor Wavelet and Local Binary Pattern features. Images dataset of 268 real H&E prostate samples collected from Shaukat Khanum Memorial Cancer Hospital & Research Centre Lahore in period of around 4 months.

Our contributions in this thesis is (*i*) collection of real prostate cancer digitized H&E sample images (*ii*) Manual grading of all images in the dataset by a team of expert pathologists (*iii*) extraction of different feature sets using Gabor filters and Local Binary Patterns with variations. *(iv)* experimental analysis of feature sets and combining most effective feature sets as single file
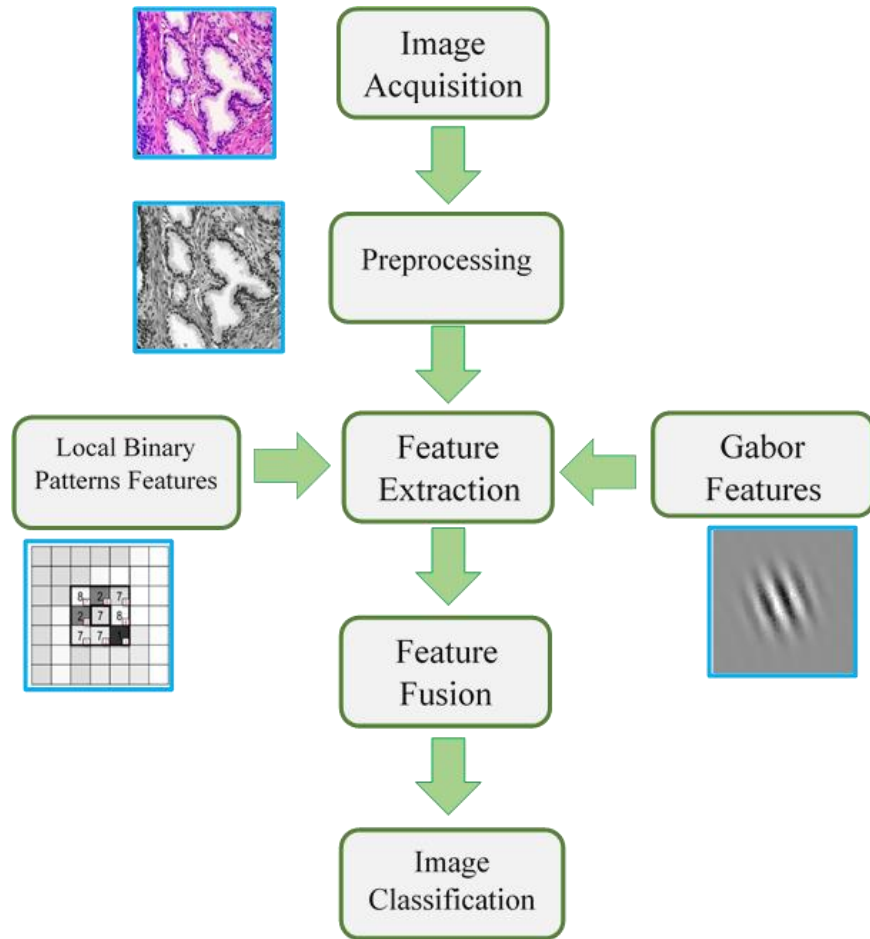
Figure 4.1: Flow diagram of the proposed system

Figure 4.1 shows flow diagram for the proposed system. H&E stained prostate samples are acquired with high resolution camera. Image slides are prepared using different magnification levels. In our case we have used images taken on 20x and 40x magnification levels. Once image is acquired, all the images are resized on some uniform level & then converted to gray-scale which will reduce the computational cost. After pre-processing, texture features are extracted using Gabor filter and Local Binary Patterns techniques as shown in the figure. Once features are extracted using different techniques, then classification is applied. Features showing better classifications results are then combined to enhance the accuracy as shown in figure. K-NN and SVM classifiers are used in this work.

4.2   Data Acquisition

Prostate cancer database collection was one of the most challenging task we have faced in this work. It took more than 3 months and hard work to get some real sample images. We have contacted multiple research groups working in same domain, laboratories and cancer hospitals by different means, but they excused due to ethical issues or data providing policies. I contacted Shaukat Khanum cancer research hospital, Lahore and they rejected my request by saying that we cannot provide you patients data due to ethical issues. We again contacted the same with an official letter from department guaranteeing the hospital that we will use this data surely for this research work. I personally visited the hospital multiple times and met Dr. Omer Waqas, pathologist at Shaukat Khanum hospital who understood the need for computerized cancer grading system. They also appreciated our work for the welfare of the cancer patients. He with his team helped us a lot and provided H&E stained prostate images. Initially they provided 35 graded images then 233 within period of two months. We trained and tested our system for 268 real samples.

The prostatic tissue samples used in this study were prepared from surgically collected biopsies after chemical processing by cutting into very thin sections of less than $5\mu m$ thickness using sharp blades. These thin slices were kept on positively charged glass slides for a whole night and then stained with Hematoxylin and Eosin (H&E) dye using an automatic staining processor. Prostatic tissue samples were acquired at different magnification levels (10x, 20x and 40x) using Olympus BX-43 up-right microscope, ProgRes, SpeedXT core 3 high resolution CCD camera and system for image acquisition and analysis. 231 prostatic adenoma images were collected in 3 months and compressed using JPEG compression with resolution of 2448×3264 pixels. Applied three approaches to reduce inter-and intra-observer variations which can increase error probability in classification: *i)* All images were analyzed and manually graded by minimum 3 experienced pathologists in a reputed Cancer hospital of Pakistan and cancer grade labeling was done manually according to Gleason grading; *ii)* Primary grade is assigned if that grade is present on more than 70% portion of the total sample. *iii)* All digitized pathological images were captured under the same technology and illumination conditions.

Grade 1 and 2 patterns were considered in the same class as these patterns were very rare. Our image dataset was divided into five categories including benign samples, grade $1 - 2$, grade 3,

grade 4 and grade 5. There are 18 benign images, 38 images in grade-1 and 2, 69 images in Grade-3, 74 images in Grade-4, and 69 images in grade-5 as shown in table 4.1.

Table 4-1: Summary of images in dataset

Grades	Number of samples
Healthy samples	18
1 & 2	38
3	69
4	74
5	69
Total	*268*

Gleason grading was performed according to guidelines provided by World Health Organization (WHO) and International Society of Urological Pathology [40].

4.3   Image Feature Extraction

The accuracy of any classification algorithm is highly dependent on the uniqueness and uncorrelation between the extracted features. So, feature extraction plays primary role in any classification system. Features can be divided into major three categories i-e Color, Texture and Shape based features [43]. We have used texture features in this work which performed well in our case.

4.3.1   Feature Extraction using Gabor Filter

Gabor filters [44] are most commonly used for image texture feature extraction. Gabor filter samples the entire frequency range of an image by central frequency and orientation parameters. An image is filtered with Gabor filters (GF) bank of different frequencies and orientation degrees. Energy is captured for each frequency and direction of the filter and feature vector is created based on energy distributions [45]. GF has a significant role in addressing several computer vision problems due to its localization properties in space and frequency. Two principle qualities of GF, band pass nature and directionality make it like mammalian cells of visual cortex and it has invariant response against scale and orientation in textures. GF is

25

composed of elliptical Gaussian function and complex sinusoidal function that makes band pass filter in frequency domain. Its mathematical expression and visual representation are given as in equation 4.1 and figure 4.2 accordingly.

$$g(x, y) = \left(\frac{1}{2\pi\sigma_x\sigma_y}\right) \exp\left(-\frac{1}{2}\left(\frac{x^2}{\sigma_x^2} + \frac{y^2}{\sigma_y^2}\right) + 2\pi j W x\right) \qquad 4\text{-}1$$

where 'W' represents centre frequency that is controlled by frequency of complex sinusoid and standard deviation (STD) of Gaussian controls bandwidth. Fourier transformation for above equation 4.1 can be illustrated as below

$$G(u, v) = exp\left(\frac{1}{2}\left(\left[\frac{(u - C)^2}{\sigma_u^2} + \frac{v^2}{\sigma_v^2}\right]\right)\right) \qquad 4\text{-}2$$

where, $\sigma u = 1/(2\pi\sigma x)$ and $\sigma v = 1/(2\pi\sigma y)$ respectively. Gabor Filter (GF) bank exhibits number of band pass filters with varying orientations, resolutions and bandwidths, whereas these are controlled by its parameters. For a certain texture real parts, magnitudes and kernel of GF are represented in figure 4.3, in which Gabor kernels are produced using two scales α=2 and 5, two orientations θ = 0.785 and 1.571 and two frequencies f = 0.5 and 2. Figure 4.2 (a) and (b) give real parts of Gabor frequency responses and Gabor kernels for above parameters respectively while (c) and (d) are magnitude and phase responses of GF for a given texture respectively.
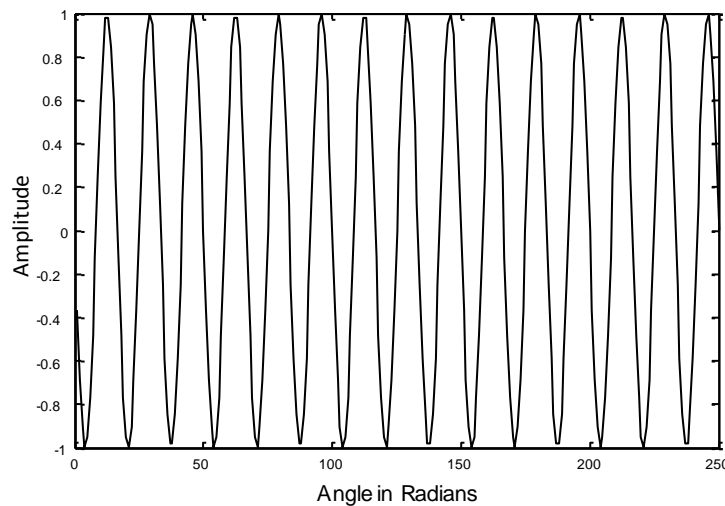
(a)
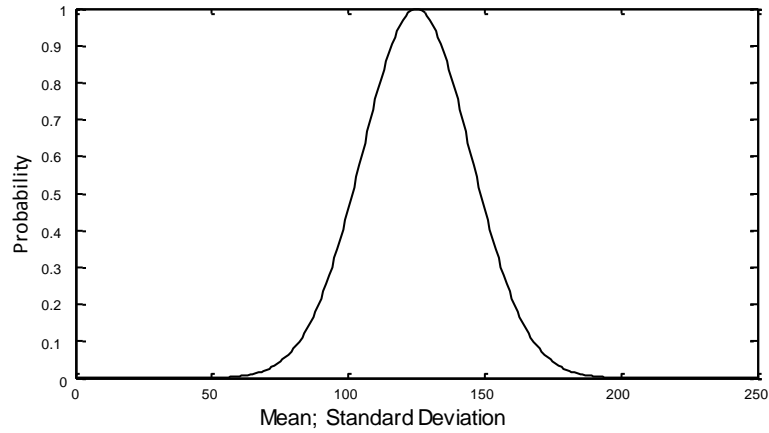
(b)
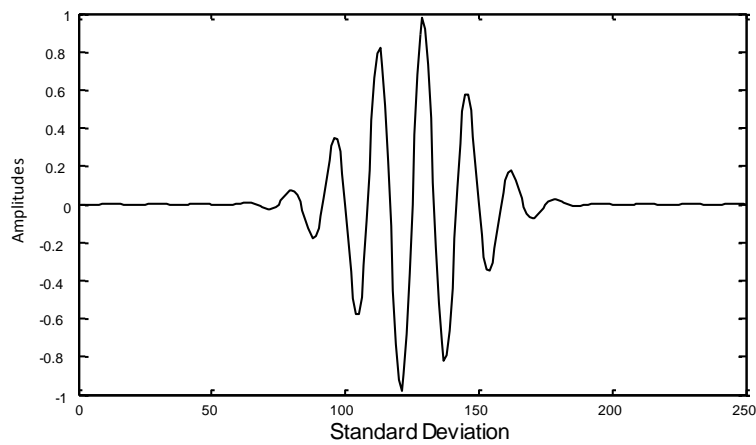
(c)

Figure 4.2: Gabor Filter's a visual presentation
(a) sinusoidal function (b) Gaussian curve and (c) Gabor Filter graph

Gabor functions form a complete and non-orthogonal set of basic functions and any given function can be expanded in terms of these basis, because the expansion gives frequency localization for texture analysis and compression. However, a localized frequency distribution is not suitable for features because this distribution needs fixed spatial window which makes bandwidth constant on linear scales.
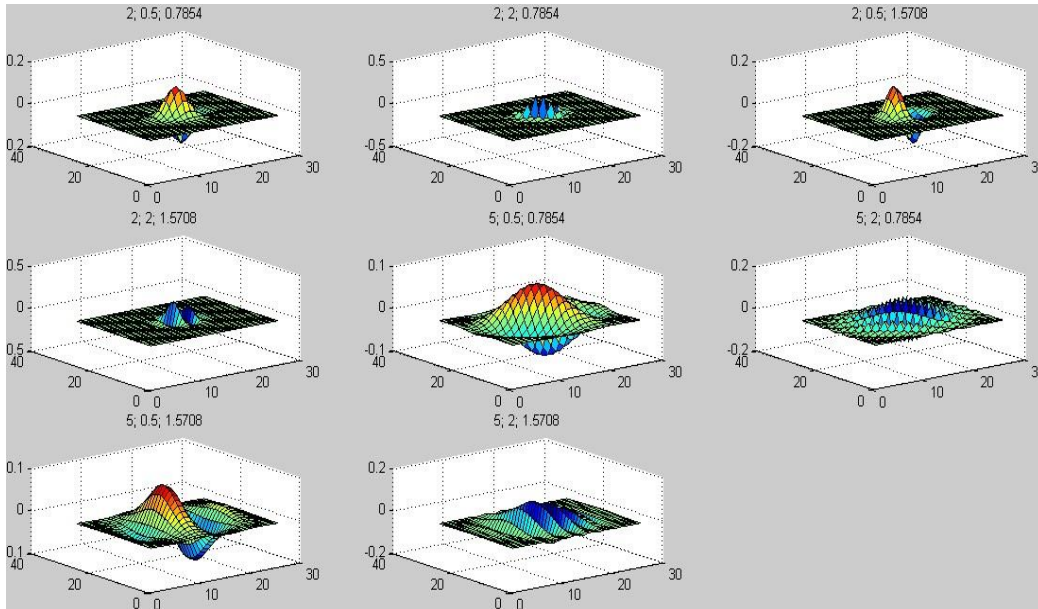
(a)
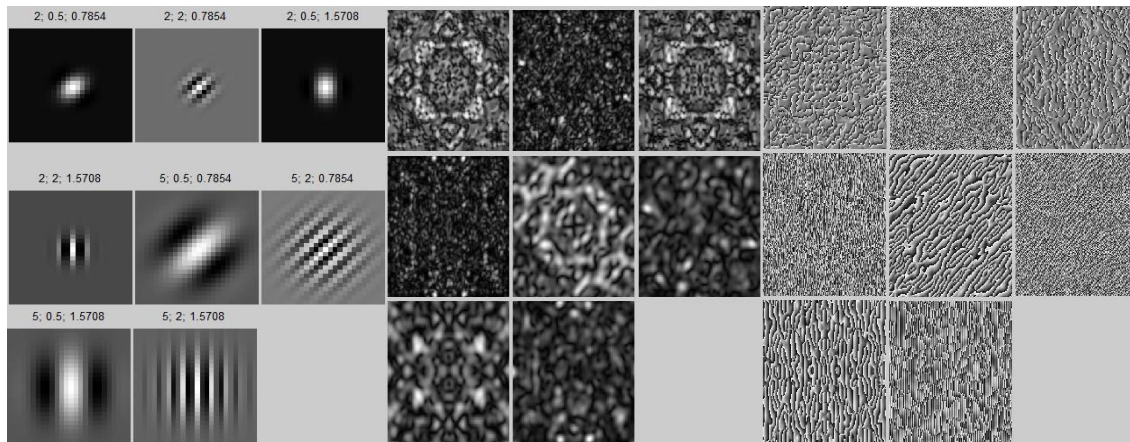
(b)   (c)   (d)

Figure 4.3: Gabor Filters constructed using different parameters (f, θ, α)

(a) Real parts of Gabor frequency responses (b) Gabor kernels for θ=45 & 90, a=2 & 5 (c) magnitude of Gabor responses for given texture (d) Phases of Gabor filter responses for given texture

For an optimal feature localization on different scales filters are required which have varying support. This leads to decomposition of wavelets in which Gabor function is basic wavelet. A GW is a complex planer which is restricted by a 2D Gaussian envelop and its ratio of width and wavelength is only thing that differentiates two GWs other than scale and orientation. A given texture image is convolved with GW in order to estimate the magnitude of local

frequencies of respective wavelength and orientation. GW is a group of mutual similar Gabor functions which are constructed by dilation and shifting from an elementary Gabor function or mother wavelet. Fig. (4.3) shows construction of Gabor filter using different parameters as frequency (f), standard deviation (α), orientation of the normal to the parallel strips (θ) of the Gabor function. Real parts in frequency response is shown in fig. 4.3 (b). Magnitude and phases response of texture is shown in (c) and (d)

An input image $I(x, y)$ is convolved with a complex conjugate ψ^* of mutual similar function constructed by mother wavelet $g(x, y)$ and a discrete wavelet transform is achieved as given in Eq. (4.3)

$$G_{pq}(x, y) = \sum_s \sum_t I(x - s, y - t)\psi^*_{pq}(s, t) \qquad 4\text{-}3$$

where p and q give value of scale and orientation respectively and s, t are variables of filter mask size and ψ is a self-similar function defined by equation (4.4)

$$\psi(x, y) = \left(\frac{1}{2\pi\sigma_x\sigma_y}\right) exp\left(-\frac{1}{2}\left(\frac{x^2}{\sigma_x^2} + \frac{y^2}{\sigma_y^2}\right) + 2\pi jWx\right) \qquad 4\text{-}4$$

While the generating function due to which wavelets are obtained is described by the following equation:

$$\psi_{pq}(x, y) = a^{-p}\psi(\bar{x}, \bar{y}) \qquad 4\text{-}5$$

Where, $\bar{x} = a^{-p}(xcos\theta + ysin\theta)$ and $\bar{y} = a^{-p}(-xsin\theta + ycos^\theta), p = 0, 1 \dots P - 1, q = 0, 1 \dots Q - 1$. P and Q numbers of scales and orientations respectively while 'α' is scaling factor. In this work, 30 Gabor mean amplitude and 30 Gabor energy distribution features for each of the sample image available in the dataset are extracted.

4.3.2 Feature Extraction using Local Binary Patterns (LBP)

Local Binary Pattern (LBP) is a structural texture descriptor which is computationally very discriminative to texture features, efficient and has made much progress in the areas of image processing, machine vision and pattern intelligence [46]. Local binary patterns (LBP) are based on two complementary measures i-e contrast and patterns of a texture image [47]. Development of LBP operators is classified into four fundamental phases [48] *i)* Introduction of

basic LBP descriptor, *ii)* Development of extensions, generalizations and theoretical background of LBP, *iii)* Introduction of LBP's applications for face description and recognition *iv)* Spatial and temporal LBPs for motion and activity analysis. Basic LBP was developed during early 90's based on the concept that two local complementary measures can describe two-dimensional texture. As part of comparative analysis of texture operators LBP work was first published in 1994 in an international conference on pattern recognition [49]. Few years later it was found that census transform proposed for computation of correspondences in stereo matching has similarity with LBP operator and both are developed in almost the same time [50]. Later LBP techniques were developed and utilized for segmentation of unsupervised segmentation of textures [51] and the results obtained clearly outperformed all other state of art techniques of that time and motivated LBP operator for further research computationally. LBP is much simpler, discriminative and efficient local operator for textures. Towards various pattern recognition and machine intelligence problems regarding texture analysis, LBP has made much impact and progress than any other technique.

Original LBP was explored and searched by Timo Ojala [51] and [52] for description and analysis of textures and other applications. Researchers in early publications did not present very high and error free precision and accuracy for segmentation and classification of textures. However, they provided a base of LBP to researchers of pattern analysis and image processing areas who explored and developed several extensions of LBP for many applications such as classification, segmentation, retrieval and object detection.

In a texture $I(x, y)$, LBP values are computed based on the neighbouring pixels by setting a threshold as shown in fig. (4.4). Mathematical expression in equation 4.6 illustrates original LBP pattern computation while a visual representation is given by figure 4.4.

$$LBP_{P,R} = \sum_{p=0}^{P-1} s(g_p - g_c).2^p \qquad 4\text{-}6$$

where,

$$s(g_p - g_c) = \begin{cases} 1 & if\ x \geq 0 \\ 0 & if\ x < 0 \end{cases}$$

In above equation LBP values are computed threshold which is based on values of central pixels g_c values having coordinates $(0,0)$ and neighbouring pixels g_c with coordinates $(x + Rcos(2\pi p/P), y - Rsin(2\pi p/P))$. For a defined number of neighbours 'P' and radius 'R' a complete binary pattern is achieved by setting '1' if g_c has lesser value than g_p or else setting value '0'. Radius and number of neighbouring pixels are user defined and can be increased or reduced, however by default LBP algorithm uses radius of '1' and '8' neighbours as shown in figure 4.4.

164	30	99	1	0	0
200	150	177	1		1
83	215	20	0	1	0

	169	
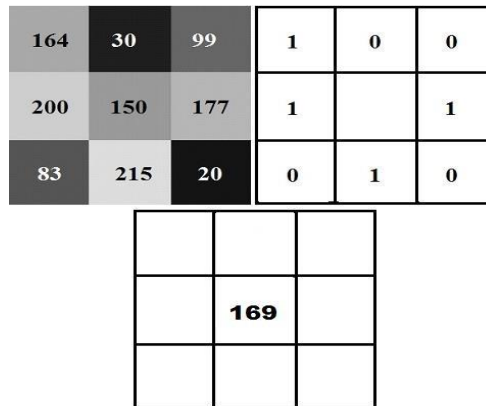
Figure 4.4: An LBP illustration using (8 neighbours with radius 1)

a) central & neighbouring pixel values b) binary pattern after LBP c) LBP value for respective neighbours

LBP for an 8-neighborhood gives about 2^8 levels as shown in fig. (4.4). Its simplicity of computation and invariance against scale and rotation differentiate it from other state of art texture descriptors. Following variants of LBP are used for extraction of more efficient features. Original LBP itself has no invariance properties but some of its extensions like $DRLBP$, $riLBP$, $riuLBP$ exhibits invariance property.

Table 4-2: Number of features extracted using different techniques

Techniques	No. of features
LBP	256
riLBP	36
riuLBP	10
DRLBP	256
riLBPV	352
Gabor Filter	30

As we have already achieved invariance properties for our experiments using Gabor descriptor and no more invariance is needed so we have used a simple non-variant extension, uniform-LBP. Number of features extracted by different techniques are shown in table 4.2. Rotation Invariant Uniform Local Binary Patterns (riuLBP) extracted lowest features set of 10 against each sample image. In our database, there are 268 images so riuLBP features vector space will consist 2680 features in total.

4.3.2.1 LBP variants

Local Binary Pattern (LBP) are texture descriptors which have been used in areas of image processing, machine vision and pattern intelligence [46]. There are different variants proposed in literature as rotation invariant, uniform, dominant rotated or combination two or more. Uniform Local Binary Patterns are those which are based on number of bit-wise transitions from zeros to ones or vice-versa [48]. These can be defined as patterns which have at most two-binary bit wise transitions from '0' to '1' and vice versa. For instance, patterns 00000011 and 01111100 have 1 and 2 transitions respectively are uniform, while 100100000 and 11101101 are non-uniform patterns that contain 3 and 4 transitions respectively. Mathematically uniform LBPs can be computed using Equation 4.7, while figure 4.4 presents a visual description of uniform patterns for a 3×3 neighbourhood, where 'n' and 'r' describe umber of ones increasing downward and left to right bitwise circular shift respectively. In experiments, we used uniform patterns due to two basic reasons, firstly maximum of LBP patterns are uniform about 90% and 70% patterns are uniform in 8 and 16 pixels neighbourhood respectively, while rest of patterns are very few and non-uniform. Second reason is that these patterns for many applications have better recognition results than other descriptors.

$$U(LBP_{P,R}) = \left| s(g_{p-1} - g_c) - s(g_0 - g_c) \right| + \sum_{p=1}^{P-1} \left| s(g_p - g_c) - s(g_{p-1} - g_c) \right| \qquad 4\text{-}7$$

If in above equation 4.7, $U \geq 2$ then pattern belongs to uniform, otherwise non-uniform family. Number of Uniform patterns for 'P' neighbourhood can be calculated by formula: "$P \times (P-1) + 3$". 256 local binary patterns, 10 Rotation Invariant Uniform Local Binary Patterns (riuLBP), 36 rotation Invariant LBP (riLBP) and 256 Dominant Rotated LBP (DRLBP) features are extracted for each image in the dataset. The extracted features numbers mentioned for Local Binary patterns variants are with '1' radius and '8' neighbours.

LBP cannot perform well if input texture image is rotated or scaled by some factor. Ojala [52] proposed a novel extension of LBP operator by using rotation invariance technique. They added invariance to the technique in a way that it can classify without affecting the results even when textures are rotated. Results were compared with state of art model based approach which was much better. Features were extracted using bilinear gray level interpolation in a window of 3x3 neighbourhood. First, they mapped decimal values into binary, then defined some indices for representation of binary patterns. e.g. 3x3 neighbouring pixels, about thirty-six patterns existed where each pattern was represented by index 0 to index 35 and that index number of matching pattern was used as feature value. Ojala [54] also proposed rotation invariant properties based on their previous work with better performance. They developed a mathematical model for invariance against rotation and orientation of textures. They trained classifier using textures at one orientation angle and tested using some other arrangement. While using indices of different patterns they proved that for an 8-neighborhood all zeros having index number 0 detected bright spots while index number 4 and 8 represented edges and dark spots in textures.

Researchers also classified LBP patterns into uniform and non-uniform. Uniform patterns are those which have two or less transactions in binary bits from 0 to 1 or vice versa where non-uniforms are those having more than two transactions. Most of authors only used uniform patterns because 90% of patterns are covered and they discarded non-uniform patterns due to simplicity and avoiding unnecessary features. In article [55] same case is applied to minimize feature vector size. The proposed work has a couple of features sets, Dominant Local Binary Patterns (DLBP) which aimed to capture most frequently occurred features of texture surfaces. Gabor based features that aimed to supply additional texture information to attributes vector. Some standard databases were used for testing classification accuracy and performance of algorithm. They separately used algorithm on texture databases and compared accuracy with other state of the art methodologies. For some databases, features from other techniques were also combined with DLBP to improve the accuracy.

4.4   Features Fusion

Multiple feature sets were extracted for using different Gabor filter and Local Binary Patterns with variants. We have applied K-NN [56] and SVM on all feature sets and recorded the classification results which are discussed in chapter 5. To improve overall accuracy of the

system, different feature set combinations are created and again classifiers are applied. This enhanced the overall performance of the system. Gabor Energy feature set combined with riuLBP with radius 1 and level 3 shows the maximum accuracy for Gleason grading. After creating combined feature sets, different classifiers are applied to test the grading accuracy.

Table 4-3: Features set after combining Gabor and LBP variants

Combined Techniques	Features Extracted
riLBP (8,1) & Gabor Energy	66
Gabor Energy & Gabor Amplitude	60
DRLBP (12,3) & Gabor Energy	286
riuLBP (8,1) & Gabor Energy	40
riLBP (8,1) & Gabor Amplitude	66
riuLBP (16,1) & Gabor Energy	4146

Table 4.2 shows the number of features extracted against each sample in the dataset. Rotation Invariant Uniform Local Binary Patterns (riuLBP) with Gabor energy techniques uses highest number of features and riuLBP with Gabor energy technique requires lowest features set as shown in table 4.3.

4.5   Classifiers

There is large number of classifiers which can perform differently in different environments. Classification accuracy of our proposed technique is observed using K-nearest neighbour (KNN), Support vector machine (SVM) and Random forest classifiers. All the classifiers are discussed below

4.5.1   K-Nearest Neighbor (K-NN)

K- Nearest neighbour algorithm is a simple non-parametric algorithm that has been used for pattern recognition and statistical [57]. It stores all samples and classifies on the bases of distance measures (Euclidian or Chi-square distance etc.). It classifies any data based on majority

votes of its neighbours by first measuring distance to each training sample, finds k nearest points and then predicts the class that is most common among 'k' points.

Figure 4.5 represents KNN classifier algorithm for two classes based on two features while central larger circle gives a ball to be put in one of two classes. Class A contains soccer balls with high weight and more circumference whereas class B has cricket balls with low weight and circumference. If 3 neighbours are considered, then central larger circle has two closest neighbours from class A and only one neighbour from class B and thus belongs to class of soccer balls. Euclidian distance is used to specify nearest neighbours and can be computed using equation 4.8 where C and W represent circumference and weights of each ball. Euclidian distance can also be computed for multiple features as equation 4.9 illustrates this for four features (i-e. radius and volume along with circumference and weight). K-NN is simple and surprisingly good classifier, however it needs to store whole training set leading to poor efficiency regarding memory.

$$d = \sqrt{(C - C1)^2 + (W - w1)^2} \tag{4.8}$$

$$d = \sqrt{(C - C1)^2 + (W - w_1)^2 + (R - R_1)^2 + (V - V_1)^2} \tag{4.9}$$
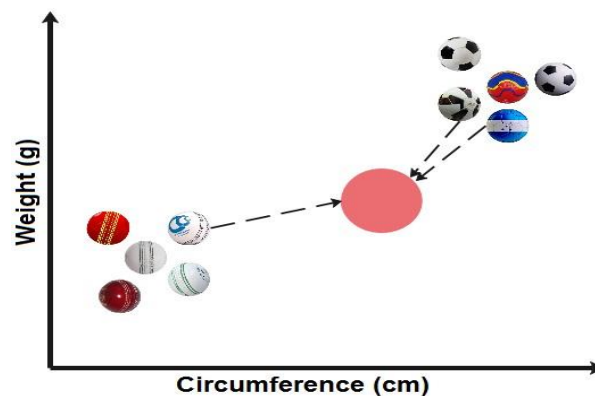
Figure 4.5: K-NN graph using 3 nearest neighbours & arrows shows distance [54]

4.5.2 Support Vector Machine (SVM)

Support Vector Machines (SVMs) [58] are sets of supervised learning algorithms proposed commonly for several machine learning and pattern recognition applications and particularly used for classification and regression purposes. These are effective and efficient for classes where number of samples is lesser compared to number of dimensions. It is also memory

efficient than KNN because it uses only a subset of training points rather than storing entire data. For decision functions, several kernel functions are specified which shows its versatile characteristics. SVM categorizes objects or classes based on construction of hyper-planes that minimizes margins among given classes or objects. The vectors that define hyper-plane are known as 'support vectors'. It classifies objects linearly through construction of a straight line between classes and largest separability among classes is achieved for largest distance of hyper-plane from training data point. A non-linear separability can also be achieved by constructing a hyper-plane and employing a repetitive training algorithm to minimize error function. All parameters are set by default in WEKA. Kernel is the most important function for SVMs which ensure the similarity and general analysis of relations like classification, clustering, correlation and rankings among data samples.
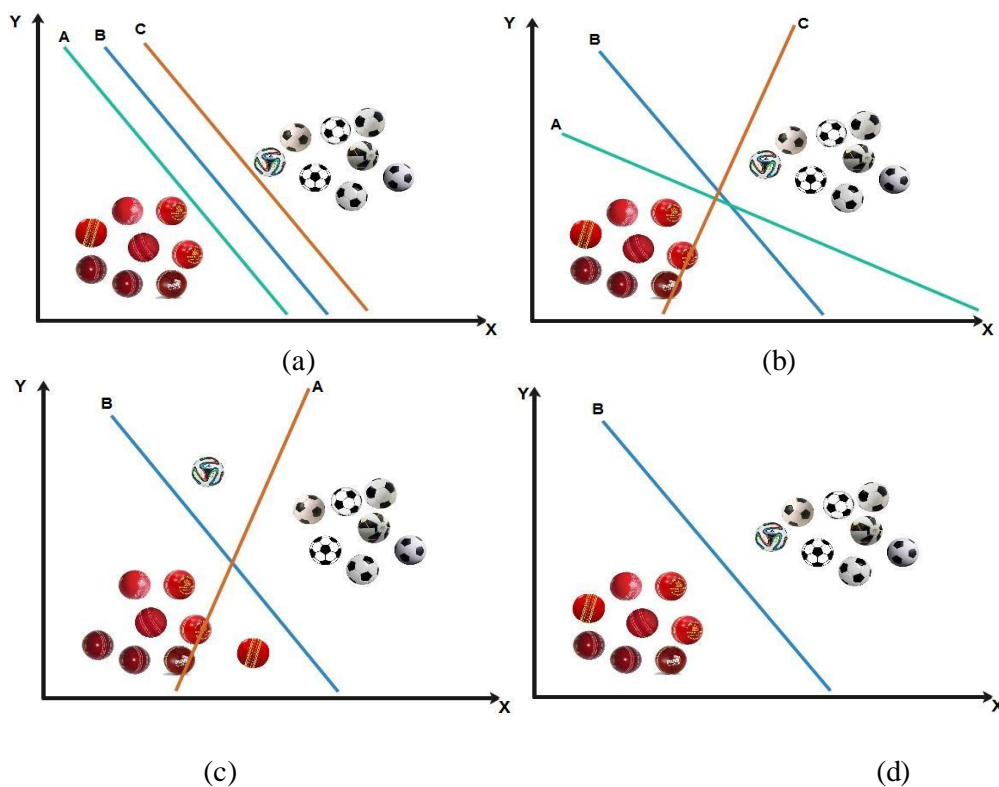
Figure 4.6: SVM different scenarios to specify right hyper-plane for separation of classes (a) Hyper-planes in same direction and different distances from classes (b) Hyper-planes in different directions (c) Hyper-planes when position of some neighbours changed and (d) Right hyper-plane to separate two classes [59]

We utilized polynomial kernel algorithm for our analysis because it is set by default and secondly it represents correlation of training samples allowing both linear and non-linear models on polynomials of variables. Best hyperplane separates classes and have maximum distance from its closest neighbours. Figure 4.6 describes different scenarios to specify right hyper-plane. Among all scenarios hyperplane B is the right one to separate two classes. There are total three hyper-planes at different distances from two either classes with same direction. (d) shows mixed class objects while has a perfect hyper-plane representing right distances from both classes.

4.5.3 Random Forest

Random forest or Random Decision Forest (RDF) algorithm works as a large collection of decorrelated decision trees. It grows a forest of many trees in which each tree may have different data and predictors. Random forest tree is different from other decision tree because it uses multiple decision tress for performing a single classification. The basic idea behind random forest is that most of the trees are good for most of the data and make mistakes in different places. It performs well for both classification and regression. It can handle categorical predictors naturally. Random forest can handle highly non-linear interactions and classification boundaries even if some variables values are missing. RDF classify feature vector using all trees where each tree votes for a class and a class with majority votes is selected. Decision trees have poor performance when used for large databases so it is replaced by random forest.

(a)

(b)
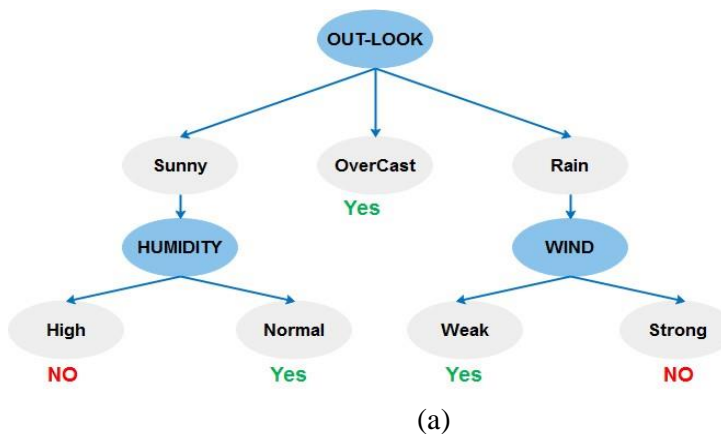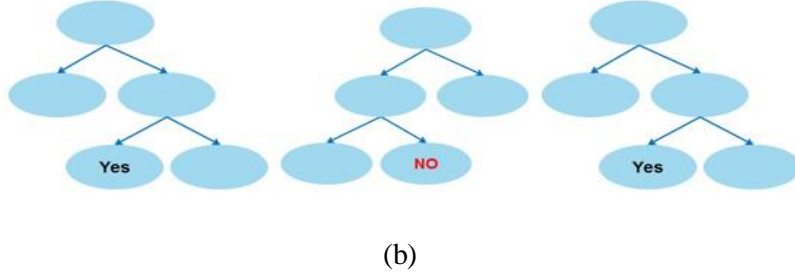
Figure 4.7: Random forest decision trees

(a) Original decision tree (b) decision trees for an unknown instance

RDF is more efficient than typical decision tree classifiers and very effective for large databases even it can handle thousands of features without deleting a single feature. Random forest works by creating multiple decision trees then predict each class by using decision tree and finally predict class with majority votes. Consider *'S'* represents data features whereas S_1, S_2 and S_3 are random subsets of original data then three decision trees for each subset would be created.

$$S = \begin{bmatrix} fA_1 & fB_1 & fC_1 & \cdots & C_1 \\ \cdot & \cdot & \cdot & & \cdot \\ \cdot & \cdot & \cdot & & \cdot \\ \cdot & \cdot & \cdot & & \cdot \\ fA_N & fB_N & & & C_N \end{bmatrix}$$

$$S_1 = \begin{bmatrix} fA_{12} & fB_{12} & fC_{12} & \cdot\cdot & C_{12} \\ fA_{15} & fB_{15} & fC_{15} & & C_{15} \\ \cdot & \cdot & \cdot & & \cdot \\ \cdot & \cdot & \cdot & & \cdot \\ fA_{35} & fB_{35} & fC_{35} & & C_{35} \end{bmatrix} S_2 = \begin{bmatrix} fA_2 & fB_2 & fC_2 & \cdot\cdot & C_2 \\ fA_6 & fB_6 & fC_6 & & C_6 \\ \cdot & \cdot & \cdot & & \cdot \\ \cdot & \cdot & \cdot & & \cdot \\ fA_{20} & fB_{20} & fC_{20} & & C_{20} \end{bmatrix} S_2 = \begin{bmatrix} fA_4 & fB_2 & fC_2 & \cdot\cdot & C_2 \\ fA_9 & fB_9 & fC_9 & & C_9 \\ \cdot & \cdot & \cdot & & \cdot \\ \cdot & \cdot & \cdot & & \cdot \\ fA_{12} & fB_{12} & fC_{12} & & C_{12} \end{bmatrix}$$

Figure 4.7 contains examples of decision trees for table 4.6, where three separate trees are created which predicts *'Yes'* or *'No'* for unknown instance and then predicts a class with majority votes. Figure 4.7 (a) is original trained decision tree diagram for data expressed in table 4.6, while figures (b) represent different decision trees. Two out of three trees predict *'Yes'* and one gives *'No'* thus random forest predicts class *'Yes'* due to majority votes.

4.6   Experimental Setup

To achieve final classification accuracy, the data set is first divided into training and testing samples. Each of the sample set is used to train and test the classifier respectively. Our experiments use two options to train and test the classifiers, one is 'k-folds cross validation' and other is 'percentage split'.

4.6.1 K-folds Cross Validation

It is essential to isolate training samples from testing ones and former one must not have any information about later one. There is possibility of that same samples are used for testing and training if the samples are not divide intelligently. This is called k-folds cross-validation where 'k' is an integer.
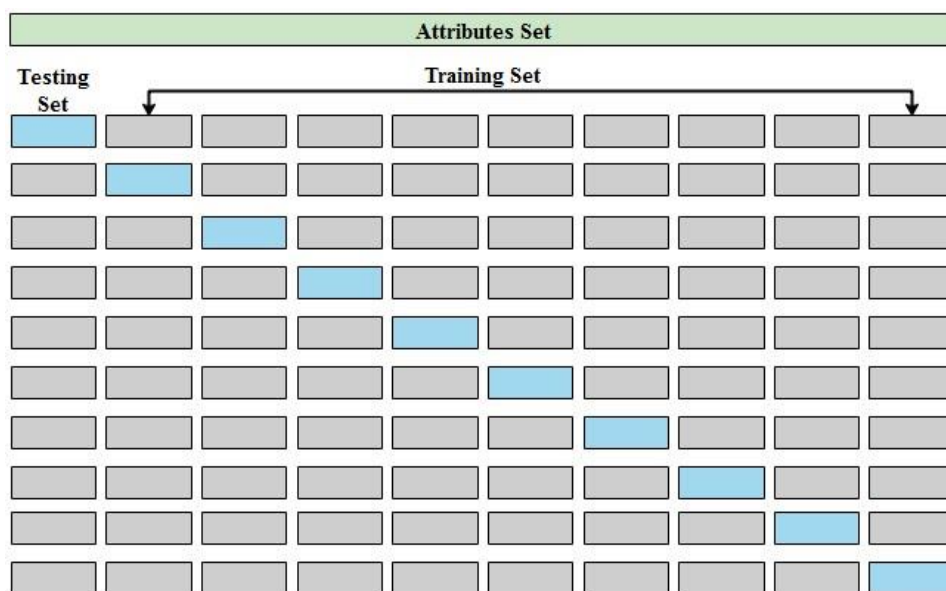
Figure 4.8: 10 Folds Cross validation, blue sets represent testing & other training sets [54]

We have applied 10-folds cross validation i.e. whole feature set is split into 10 equal subsets or folds with samples of each class. Nine folds are used for training while the remaining one is a test set. Ten iterations are required so that each time different folds are used for training and testing sets. Thus, after obtaining results for 10 times, their average is taken and used as the result of classification. Illustration is given in figure 4.8.

Percentage split refers to partition of data into training and testing subsets by a specific ratio. We have also tested our algorithm by splitting the dataset into different percentage combinations for 50-50, 70-30, 60-40 training and testing samples respectively. We have used Weka toolkit [5] for implementing classifiers, in which there is an option to set percentage split of data for training and testing purpose with k-cross fold validation.

4.7   Summary

This chapters shows our proposed methodology of Prostate Gleason grading system. All the steps involved in developing the algorithm is explained in detail. The technical process of making real samples is discussed in detail. Feature extraction using Gabor wavelets and Local Binary patterns are discussed in detail. K-NN, SVM and Random forest are used to test the grading accuracy on individual feature sets. Then to enhance the overall performance of the system, different feature sets are combined on experimental basis. The most challenging task was to collect real H&E stained prostate cancer sample images dataset.

CHAPTER 5:   EXPERIMENTAL RESULTS

This chapter explains complete experimental procedures used to validate the results. It is divided into two major sections as experimental results and comparison with other state of art techniques. All the extracted features against different techniques with achieved accuracies are discussed in detail. K-NN, SVM and Random Forest classifiers are used to validate the results. Maximum accuracy as compared to other state of the art techniques is achieved by combining Gabor & local binary patterns.

5.1   Prostatic Dataset & Preprocessing

The efficiency of the proposed Gleason grading system is tested on the real sample images obtained from Shaukat Khanum Memorial Cancer Hospital & Research Centre Lahore and few images available on web pathology [60]. There are 268 coloured images of different size in our dataset. There are 18 benign, 38 grade-1 and 2, 69 grade-3, 74 grade-4 and 69 grade-5 grayscale images. Grade-1 & 2 were not considered for grading because these are considered as benign and requires no treatment according to physicians. The images in the dataset were in different size, so all the images are converted to gray scale and resized to 512*512 pixels. The proposed system can classify between benign vs malignant tissues and can grade between 3,4 & 5 grades.

5.2   Tools Used

The proposed prostate classification system is implemented and evaluated using MATLAB 2013a and Weka 3.6. MATLAB is used to implement different techniques for feature extraction. The extracted features are saved in .csv format. Weka [5] is used to apply different classifiers to evaluate the accuracies using different feature vectors. 10-fold cross validation is used in Weka while classifying to validate the results more effectively.

5.3   Results and Discussions

Prostate cancer classification literature shows that texture features can perform well in Gleason grading because Gleason standard is based on the texture distribution. We have extracted large number of feature sets implementing Gabor wavelets and Local binary patterns with some variants. LBP results are shown for different levels 'p' and Radius 'r'. K-NN, SVM

and Random forest classifiers are applied in Weka to get the results which are presented in table 5.1 in detail.

Table 5-1: Results Achieved by Gabor Filter & LBP Variants using 10-fold cross validation

Technique	Radius	K-NN			SVM			Random Forest		
		Accuracy (%)								
		p=8	p=12	p=16	p=8	p=12	p=16	p=8	p=12	p=16
LBP	r=1	82.17	80.13	80.11	71.4	69.0	63.2	78.2	77.4	74.9
riuLBP	r=1	**84.34**	83.35	84.18	61.3	63.4	64.3	82.1	83.9	81.7
	r=3	76.96	80.43	82.61	61.3	64.7	75.2	80.4	82.6	80
riLBP	r=1	82.61	66.09	60.87	75.6	63.0	53.9	80.8	80	73.9
	r=3	80.87	80.87	70.43	75.2	69.5	52.1	78.6	81.3	72.1
DRLBP	r=1	80.43	63.04	74.78	70	53.4	58.2	82.1	73.9	75.5
	r=3	79.57	83.74	82.61	73.9	51.3	60.1	81.3	78.6	77.8
riLBPV	r=1	82.60	68.9	53.48	70.2	63.9	58.6	80.3	70.0	66.5
	r=3	80.86	72.17	83.48	68.6	66.0	70.2	79.9	76.0	69.7
Gabor Filter	Energy	**86.09**			84.78			85.52		
	Amplitude	85.65			83.48			81.30		

It can be seen in the table 5.1 that Gabor Energy features are showing maximum accuracy of 86.03%. In our case, K-NN and SVM performed even the number of features are less. Table 5.2 shows the individual accuracies of grade-0, grade-3, grade-4 & grade-5 for Gabor wavelet energy with K-NN

Table 5-2: Average Classification rate for each class

Grade	Testing samples	Correctly Classified	Accuracy %
Grade-0	18	12	66.7
Grade-3	69	66	95.6
Grade-4	74	62	83.7
Grade-5	69	58	84.0
Total	*230*	*198*	*86.0*

The confusion matrix is considered an affective representation showing handsome details in a single table. Confusion matrix against table 5.2 is shown in table 5. 3 below for the above table is shown in table below

Table 5-3: Confusion matrix

	Grade-0	Grade-3	Grade-4	Grade-5
Grade-0	12	0	5	1
Grade-3	0	66	2	1
Grade-4	2	1	62	9
Grade-5	1	1	9	58

The overall performance of classification system depends on multiple factors as number of features, time taken by algorithm for classification, the quantity and quality of dataset and result validation. When implementing classification system, the number of features can directly affect the efficiency and performance of the system. The system with less number of features will cost low in terms of performance, accuracy and system resources. Table 5.4 presents the total number of features extracted against each sample. Gabor energy and rotation invariant local binary patterns (LBP) are performing well with minimum number of features. The accuracies in this table are evaluated using K-NN and 10-fold cross validation in Weka.

Table 5-4: Accuracy and number of features extracted against techniques with K-NN

Techniques	No. of features	Max Accuracy (%)
LBP	256	82.17
riLBP	36	82.61
riuLBP	**10**	**84.34**
DRLBP	256	80.43
riLBPV	352	82.60
Gabor Filter	30	86.09

5.3.1 Combining different Features sets

After experimentation, we come to know that different features can be combined as a single feature space to enhance the performance of the system. In this research, we have tried different feature combination to get maximum accuracy. Table 5.5 shows different combined techniques, number of extracted features and achieved maximum accuracies. It is clear that combining riuLBP (level = 8 & radius = 1) and Gabor energy features performed extremely well and having minimum number of feature space. The proposed system has achieved maximum accuracy using K-NN as classifier and 10-fold cross validation [61].

Table 5-5: Results achieved by combining Gabor and LBP Variants Using K-NN

Combined Techniques	Feature Extracted	Accuracy (%)
riLBP(p=8, r=1) & Gabor Energy	66	89.13
Gabor Energy & Gabor Amplitude	60	84.78
DRLBP (p=12, r=3) & Gabor Energy	286	81.74
riuLBP (p=8, r=1) & Gabor Energy	40	**98.60**
riLBP(p=8, r=1) & Gabor Amplitude	66	86.52
riuLBP (p=16, r=1) & Gabor Energy	4146	62.17

Figure 5.1 gives a graphical representation of results achieved from 10-fold cross validation on the dataset. LBP and Gabor experimental results are shown against K-NN, SVM and Random Forest classifiers. It can clearly be observed from the chart that in our case, simple K-NN classifier is performing very well. The advantage of the proposed system compared with others is that we achieved highest accuracy with small feature set size and computation cost.
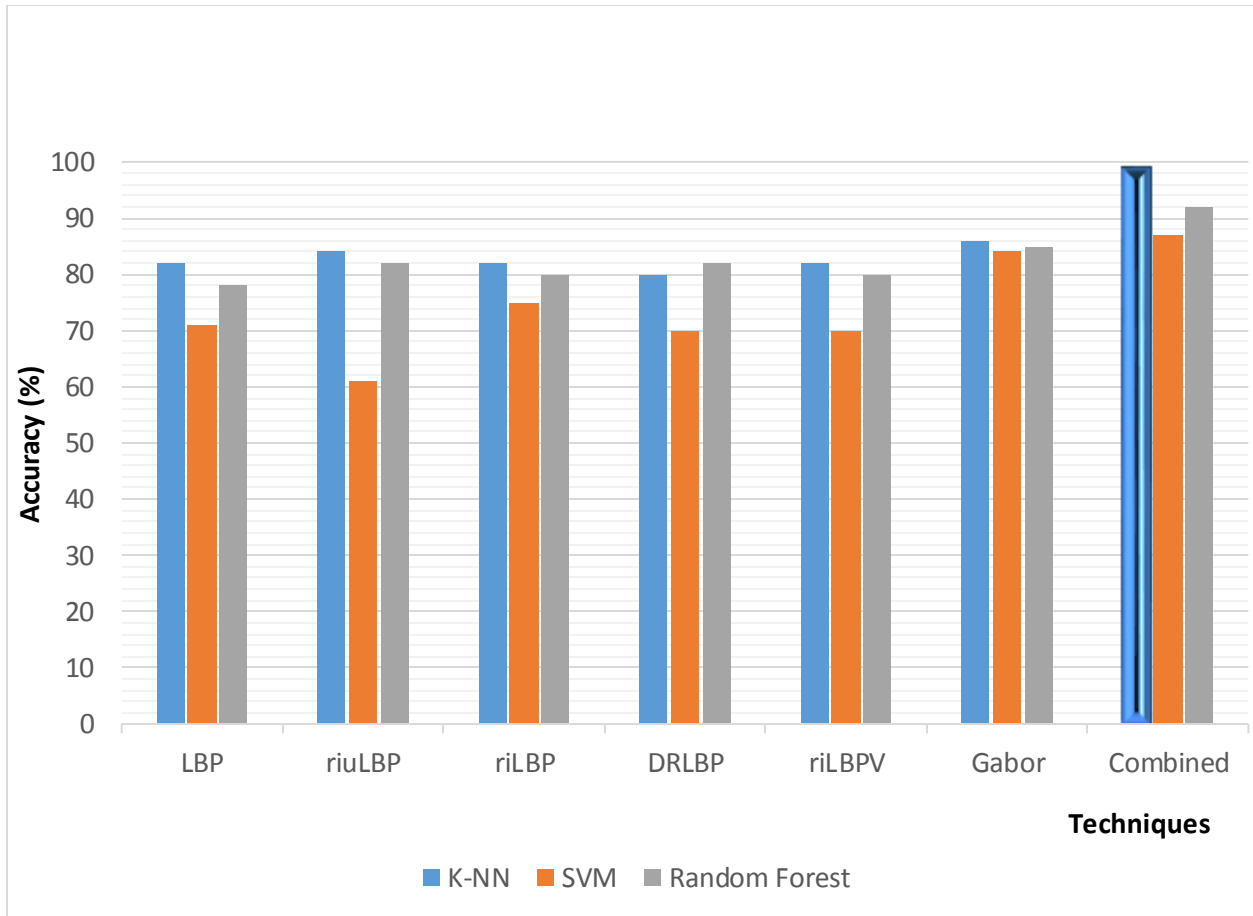
Figure 5.1: Achieved accuracies using different features and classifiers

5.4   Comparison with state of the art techniques

In this section, results are compared with other state of the art methods reported in literature. Table 5.4 enlists results achieved by several researchers for computerized Gleason grading of Prostate cancer images, which has already been discussed in literature review section. There is no prostate cancer images dataset available publicly, so different researchers used their own datasets collected from different hospitals. Different researchers have used different datasets, techniques and classifiers. Our proposed method used real dataset, extracted more than 20 feature vector sets and applied three different classifiers to validate our results. The comparison table clearly shows that our proposed method performed very well and achieved the highest accuracy with real and large dataset as compared to other studies in literature.

Table 5-6: Comparison with state of the art techniques

Authors	Year	Techniques	Classifier	Dataset samples	Accuracy (%)
Anna Gummeson et al. [62]	2017	Neural networks	K-NN	213 images	92.7
Usman et al. [63]	2016	Haar wavelet transform	SVM	129 images	92.24
Rezaeilouyeh et al. [26]	2016	Sherlet Transform	SVM	100 images	90.0
Litjens et al. [27]	2015	Color Histogram, Local Bianry Patterns	Random Forest	204 images	92.0
Mosquera-Lopez et al. [28]	2012	Structural Segmentation	SVM	71 images	87.30
Khurd et al. [15]	2010	Texton maps	Random forest	75 images	72.11
Our method [61]	2017	Gabor, Local Binary Patterns	KNN, SVM, RDF	230 images	**98.60**

5.5   Conclusion

We have proposed a robust computer aided system by combining Gabor and LBP feature sets for the grading of prostate cancer from images. We have used multiple classifiers as K-NN, SVM and Random Forest classifiers to fairly evaluate our results. On experimental basis, different extracted features vectors are combined as single feature vector file to improve overall accuracy of the system. Average accuracy is calculated by taking average of the all accuracies for 10 folds in multiple iterations. Our experimental results showed that our proposed Gabor Energy with rotation invariant local binary patterns method gives better grading accuracy as compared to other methods reported in literature.

CHAPTER 6: CONCLUSION AND FUTURE WORK

This chapter concludes the research work presented in this report. This work can be further implemented for different cancers which is discussed in future works section in this chapter.

6.1 Conclusion

Prostate cancer is a deadly disease forming the second biggest reason for cancer related deaths in men. Computer aided diagnosis for disease identification is very important specially for third world countries like Pakistan, where oncologist to patient ratio is extremely low. There may exist large variations between Grades marked by different pathologists which can lead to wrong treatment. For this reason, a uniform and practical and trustworthy computerized cancer classification system is required.

In this thesis, we have studied and implemented prostate cancer histological image grading algorithm based on Gabor wavelets and Local Binary Patterns (LBP). The accuracy of any classification system is highly dependent on uncorrelation and uniqueness between extracted features. The most challenging task was to collect real sample images, which we collected from Shaukat Khanum Memorial Cancer Hospital & Research Centre, Lahore. Our Images database consist of 268 histological H&E stained images. A team of expert pathologists at pathology department graded the images manually which is further required for training the proposed algorithm. We have extracted and saved different feature sets by varying parameters in Gabor and local binary patterns. Performed classification on extracted feature sets one by one using Weka and MATLAB. To make the system more accurate, we combined different feature sets as a single feature set. Again, applied classification on the combined feature sets, we got much improved results as discussed in results chapter. Average accuracy is calculated by taking average of the all accuracies for different folds in multiple iterations. Simple K-NN (k-nearest neighbour) classifier is used for classification of images into one of the five Gleason grades. Experimental results showed that our proposed Gabor Energy with Rotation Invariant Local Binary Patterns (riLBP) method gives highest grading accuracy as compared to other methods reported in literature. The highest achieved grading accuracy of our system is 98.60% which is much better than the similar algorithms. Thus, feature vector simplicity and highest accuracy rate differentiate our proposed method from other state off the art techniques.

6.2 Future Work

As discussed above, much of research has been conducted for classification of prostate cancer but still much research is required to make this system practical. This research and thesis will open doors for more development and improvements to enhance performance, processing speed and reduce the complexity and size of feature vectors. The purpose of this work is to help the pathologists to identify correct Gleason grade (1-5) from H&E prostate cancer samples. The work can be further extended by extracting more feature sets which will enhance overall performance of the system. Neural networks and fractal analysis can also be applied which may improve the overall performance of the system. Collecting H&E prostate samples was a great challenge in this research. Dataset can be increased to make the grading system more accurate and practical. There is much to do in detection and grading of cancers so that computerized system can lead a non- specialist doctor to identify and classify cancers confidentiality, before it can be forwarded to a specialist for further analysis. This will help to reduce the waiting span of critical cancer patients before they can be diagnosed properly and treated. We will continue this work in future and will public some of the real samples for experimental purposes.

References

[1] Siegel, Rebecca L, Miller, Kimberly D and Jemal, "Cancer statistics, 2018," *CA: a cancer journal for clinicians,* vol. 66, no. 1, pp. 7-30, 2018.

[2] S. A. Clara Mosquera Lopez, "A New Set of Wavelet- and Fractals-based Features for Gleason Grading of Prostate Cancer Histopathology Images," in *Proc. of SPIE- IS&T Electronic Imaging*, 2013.

[3] Gleason, Donald, George and Mellinger, "Prediction of prognosis for prostatic adenocarcinoma by combined histological grading and clinical staging," *The Journal of urology,* pp. 58-64, 1974.

[4] L. Cooper, A. Carter, A. Farris, F. Wang, J. Kong, D. Gutman, P. Widener, T. Pan, S. Cholleti, A. Sharma, T. Kurc, D. Brat and J. Saltz, "Digital Pathology: Data-Intensive Frontier in Medical Imaging," *Proceedings of the IEEE,* vol. 100, no. 4, pp. 991-1003, 2012.

[5] I. Russell and Z. Markov, "An Introduction to the Weka Data Mining System," in *Proceedings of the 2017 ACM SIGCSE Technical Symposium on Computer Science Education*, 2017.

[6] S. Dixon, " Sporadic Colon Cancer Definition, Risk, and Prevention," very well, 18 02 2017. [Online]. Available: http://coloncancer.about.com/od/glossaries/g/Cancer.htm. [Accessed 25 May 2017].

[7] Bali, M. Singh, Padmavathi, Khorate and Ahmed, "Malignant Fibrous Histiocytoma - An Unusual Transformation from Benign to Malignant," *Journal of Cancer Sci Ther 2,* pp. 53-57, 2010.

[8] Jedinak, Andrej, Curatolo, Simon, M. K. Bhasin, T. A and Roopali, "Novel non-invasive biomarkers that distinguish between benign prostate hyperplasia and prostate cancer," *BMC cancer,* vol. 15, 2015.

[9] Demir, Cigdem and Yener, "Automated cancer diagnosis based on histopathological images: a systematic survey," *Rensselaer Polytechnic Institute,* 2005.

[10] E. Pisick, "Cancer Treatment Centers of America," 2016. [Online]. Available: http://www.cancercenter.com/prostate-cancer/symptoms/. [Accessed 25 May 2017].

[11] A. Mescher, Junqueira's Basic Histology: 12th Revised edition, New York: Mcgraw-hill medical, 2010.

[12] Mohler, J. L, Armstrong, A. J, Bahnson, R. R, D'Amico, A. Victor, Davis, B. J, J. A. Eastham, C. A, Farrington, T. A, Higano, C. S, Horwitz and Eric, "Prostate cancer, version 1.2016," *Journal of the National Comprehensive Cancer Network,* vol. 14, pp. 19--30, 2016.

[13] D. F. Gleason and G. T. Mellinger, "Prediction of prognosis for prostatic adenocarcinoma by combined histological grading and clinical staging," *The Journal of urology,* vol. 167, pp. 953-958, 2002.

[14] M. Gurcan, L. Boucheron, A. Can, A. Madabhushi, N. Rajpoot and B. Yener, "Histopathological Image Analysis: A Review," in *IEEE Rev. Biomed. Eng*, 2009.

[15] P. Khurd, C. Bahlmann, P. Maday, A. Kamen, S. Gibbs-Strauss, E. M. Genega and J. V. Frangioni, "Computer-aided gleason grading of prostate cancer histopathological images using texton forests," *Proc.IEEE Int. Symp. Biomed. Imaging,* pp. 636-639, 2010.

[16] S. J. Keenan, J. Diamond, W. G. McCluggage, H. Bharucha, D. Thompson, P. H. Bartels and P. W. Hamilton, "An automated machine vision system for the histological grading of cervical intraepithelial neoplasia (CIN)," *Journal of pathology,* vol. 192, no. 3, pp. 651-662, 2000.

[17] A. N. Basavanhally, S. Ganesan, S. Agner, J. P. Monaco, M. D. Feldman, J. E. Tomaszewski, G. Bhanot and A. Madabhushi, "Computerized image-based detection and grading of lymphocyticinfiltration in HER2+ breast cancer histopathology," *IEEE Transaction on Biomedical Engineering,* vol. 57, no. 3, pp. 642-653, 2010.

[18] K. J, Sertel, B. K, Saltz and Gurcan, "A multi-resolution image analysis system for computer-assisted grading of neuroblastoma differentiation," *Proceeding SPIE,* vol. 6, 2008.

[19] K. Masood and N. Rajpoot, "Texture based classification of hyperspectral colon biopsy samples using CLBP," *IEEE International Symposium on Biomedical Imaging: From Nano to Macro,* 2009.

[20] Saraswathi, Sharmila and Srinivasan, "An automated diagnosis system using wavelet based SFTA texture features," in *Conference on Information Communication and Embedded Systems (ICICES), 2014 International*, 2014.

[21] Sklansky and Jack, "Image Segmentation and Feature Extraction," *IEEE Transaction on,* pp. 237-247, 1978.

[22] Haralick and R. M, "Statistical and structural approaches to texture," *Proceedings of the IEEE,* vol. 67, no. 5, pp. 786-804, 1979.

[23] Waugh, Purdie, Jordan and Vinnicombe, "Magnetic resonance imaging texture analysis classification of primary breast cancer," in *European radiology*, 2016.

[24] Xie, Jun, Jiang, Yifeng, Tsui and Hung-tat, "Segmentation of kidney from ultrasound images based on texture and shape priors," *IEEE transactions on medical imaging,* vol. 24, no. 1, pp. 45-57, 2005.

[25] Chang-ming, Guo-chang, Hai-bo, Liu, Shen and Hualong, "Segmentation of ultrasound image based on texture feature and graph cut," in *Computer Science and Software Engineering, 2008 International Conference*, IEEE, 2008, pp. 795-798.

[26] Rezaeilouyeh, Hadi, Mahoor and M. H, "Automatic Gleason grading of prostate cancer using shearlet transform and multiple kernel learning," *Journal of Imaging,* vol. 2, no. 3, p. 25, 2016.

[27] Litjens, Bejnordi, Ehteshami, Timofeeva, Swadi, Kovacs and Hulsbergen, "Automated detection of prostate cancer in digitized whole-slide images of H & E-stained biopsy specimens," in *SPIE Medical Imaging*, International Society for Optics and Photonics, 2015.

[28] Lopez, C. Mosquera, Agaian, Sanchez, Isaac, Almuntashri and Zinalabdin, "Exploration of efficacy of gland morphology and architectural features in prostate cancer gleason grading," in *IEEE International Conference on Systems, Man, and Cybernetics (SMC)*, , IEEE, 2012, pp. 2849-2854.

[29] Khurd, Parmeshwar, Grady, Kamen, G. Strauss, Summer, Genega, E. M, Frangioni and J. V, "Network cycle features: Application to computer-aided gleason grading of prostate cancer histopathological images," in *Biomedical Imaging: From Nano to Macro, 2011 IEEE International Symposium*, IEEE, 2011, pp. 1632-1636.

[30] Almuntashri, Thompson, Rabah, Danny, Al-Abdin, O. Zin, Nicolas and Marlo, "Gleason grade-based automatic classification of prostate cancer pathological images," *Systems, Man, and Cybernetics (SMC), 2011 IEEE International Conference,* pp. 2696--2701, 2011.

[31] Yoon, Hong-Jun, Ching-Chung, Christudass, Christhunesa, Veltri, Robert, Epstein, J. I, Zhang and Zhen, "Cardinal multiridgelet-based prostate cancer histological image classification for Gleason grading," *Bioinformatics and Biomedicine (BIBM), 2011 IEEE International Conference,* pp. 315-320, 2011.

[32] Tai, Shao-Kuo, Cheng-Yi, Wu, Yen-Chih, Jan, Yee-Jee, Lin and Shu-Chuan, "Classification of prostatic biopsy," in *6th IEEE International Conference on Digital Content, Multimedia Technology and its Applications (IDC)*, 2010.

[33] Gertych, Arkadiusz, Nathan, Zhaoxuan, Fuchs, T. J, Salman, Sadri, Mohanty, Sambit, Bhele, Sanica, Adriana, Amin, M. B, Knudsen and B. S, "Machine learning approaches to analyze histological images of tissues from radical prostatectomies," *Computerized Medical Imaging and Graphics,* pp. 197-208, 2015.

[34] Jafari-Khouzani, Kourosh, Soltanian-Zadeh and Hamid, "Multiwavelet grading of pathological images of prostate," *IEEE Transactions on Biomedical Engineering,* vol. 50, no. 6, pp. 697-704, 2003.

[35] Fehr, D. a. Veeraraghavan, H. a. Wibmer, A. a. Gondo, T. a. Matsumoto, K. a. Vargas, H. A. a. Sala, E. a. Hricak, H. a. Deasy and J. O, "Automatic classification of prostate cancer Gleason scores from multiparametric magnetic resonance images," *Proceedings of the National Academy of Sciences,* vol. 112, pp. E6265--E6273, 2015.

[36] Epstein, Egevad, Jonathan, B. Delahunt, Mahul, S. Brett and R. J. Humphrey, "International Society of Urological Pathology (ISUP) consensus conference on Gleason grading of prostatic carcinoma: definition of grading patterns and proposal for a new grading system," *The American journal of surgical pathology,* pp. 244--252, 2014.

[37] Kamarainen, V. Kyrki and H. Kalviainen, "invariance properties of Gabor filter-based features-overview and applications," *IEEE Transactions on image processing,* pp. 1088-1099, 2006.

[38] F. Riaz, A. Hassan, S. Rehman and U. Qamar, "Texture classification using rotation-and scale-invariant gabor texture features," in *IEEE Signal Processing Letters*, 2013.

[39] Pietikäinen, Matti, A. Hadid, G. Zhao and T. Ahonen, in *Computer vision using local binary*

patterns, vol. Vol. 40, Springer Science & Business Media, 2011.

[40] Epstein, Jonathan, Allsbrook, Egevad and L. Mahul, "International Society of Urological Pathology (ISUP) consensus conference on Gleason grading of prostatic carcinoma," *The American journal of surgical pathology,* vol. 29, pp. 1228--1242, 2005.

[41] Schwartz, W. Robson, D. Silva, R. Dutra, Davis, L. S, Pedrini and Helio, "A novel feature descriptor based on the shearlet transform," in *18th IEEE International Conference on Image Processing (ICIP)*, 2011.

[42] T. Ping and Dong, "A review on image feature extraction and representation techniques," *International Journal of Multimedia and Ubiquitous Engineering,* vol. 8, pp. 385--396, 2013.

[43] Manjunath, B. S and Wei-Ying, "Texture features for browsing and retrieval of image data," *IEEE Transactions on pattern analysis and machine intelligence,* vol. 18, pp. 837--842, 1996.

[44] Grigorescu, S. E, Petkov, Nicolai, Kruizinga and Peter, "Comparison of texture features based on Gabor filters," *IEEE Transactions on Image processing,* vol. 11, pp. 1160--1167, 2002.

[45] Mehta, Rakesh, Egiazarian and Karen, "Dominant rotated local binary patterns (DRLBP) for texture classification," *Pattern Recognition Letters,* vol. 71, no. Elsevier, pp. 16--22, 2016.

[46] Ahonen, Timo, Matas, Pietikainen and Matti, "Rotation invariant image description with local binary pattern histogram fourier features," *Image Analysis,* no. Springer, pp. 61-70, 2009.

[47] Pietikäinen, Matti, Hadid, Abdenour, Zhao, Guoying, Ahonen and Timo, Local binary patterns for still images, Springer, 2011.

[48] Ojala, Timo, Pietikainen, Matti, Harwood and David, "Performance evaluation of texture measures with classification based on Kullback discrimination of distributions," in *Proceedings of the 12th IAPR International Conference*, 1994.

[49] Zabih, Ramin, Woodfill and John, "Non-parametric local transforms for computing visual correspondence," in *European conference on computer vision*, 1994.

[50] T. Ojala, Pietik and Matti, "Unsupervised texture segmentation using feature distributions," *Pattern Recognition,* vol. 32, pp. 477-486, 1999.

[51] Ojala, Timo, Pietikainen, Matti, Maenpaa and Topi, "Multiresolution gray-scale and rotation invariant texture classification with local binary patterns," *IEEE Transactions on pattern analysis and machine intelligence,* vol. 24, no. IEEE, pp. 971-987, 2002.

[52] Ojala, Timo, Pietikinen, Matti and Topi, "Gray scale and rotation invariant texture classification with local binary patterns," *European Conference on Computer Vision,* no. Springer, pp. 404-420, 2000.

[53] Liao, M. WK, Chung and A. CS, "Dominant local binary patterns for texture classification," *IEEE transactions on image processing,* vol. 18, no. IEEE, pp. 1107-1118, 2009.

[54] Cunningham, Padraig, Delany and S. Jane, "k-Nearest neighbour classifiers," *Multiple Classifier*

Systems, vol. 34, no. Springer, pp. 1-17, 2007.

[55] Keller, James, Michael, James and Givens, "A fuzzy k-nearest neighbor algorithm," *IEEE transactions on systems, man, and cybernetics,* vol. 4, pp. 580-585, 1985.

[56] Xie and Kan, "Support Vector Machine Concept and matlab build," 2011.

[57] M. Ahmed, A. Shaukat and U. Akram, "Comparative analysis of texture descriptors for classification," in *IEEE International Conference on Imaging Systems and Techniques (IST), 2016,* 2016.

[58] D. D. Ramnani, "Adenocarcinoma of Prostate," WebPathology, [Online]. Available: http://www.webpathology.com/case.asp?case=20. [Accessed 24 04 2018].

[59] M. T. Farooq, A. Shaukat, U. Akram, O. Waqas and M. Ahmad, "Automatic gleason grading of prostate cancer using Gabor filter and local binary patterns," in *40th International Conference on Telecommunications and Signal Processing (TSP)*, Spain, 2017.

[60] A. Gummeson, I. Arvidsson, M. Ohlsson, N. Overgaard, A. Krzyzanowska, A. Heyden and Bjartell, "Automatic Gleason grading of H\&E stained microscopic prostate images using deep convolutional neural networks," in *SPIE Medical Imaging*, 2017.

[61] Usman, A. Shaukat, Masroor, Jehad, Khalil, Muhammad and M. Ali, "Automatic Cancerous Tissue Classification using Discrete Wavelet Transformation and Support Vector Machine," 2016.